https://doi.org/10.5194/egusphere-2026-2704
Preprint. Discussion started: 27 May 2026

Impact of Increased GNSS Radio Occultation Data Coverage on Tropical Cyclogenesis Prediction

Hsiao-Chun Lin, Ying-Hwa Kuo, Jan-Peter Weiss, John Braun, William Gullotta

University Corporation for Atmospheric Research, Boulder, 80307, U. S. A.

Correspondence to: Hsiao-Chun Lin (hchunlin@ucar.edu)

Abstract. This study investigates the impact of increased global navigation satellite system (GNSS) radio occultation (RO) data coverage on the prediction of tropical cyclogenesis in the North Atlantic Ocean. RO data from the Radio Occultation Modelling Experiment (ROMEX) are used to construct three datasets with varying numbers of profiles and spatiotemporal coverage. The impacts of these datasets on the genesis forecasts for six selected tropical cyclones during the 2022 Atlantic hurricane season are assessed. Results show that assimilating RO datasets with higher horizontal data density and more homogeneous spatiotemporal distribution leads to improved detection of tropical cyclogenesis. Additional model diagnosis shows that the improved prediction of cyclogenesis is associated with increased specific humidity and relative vorticity, which support stronger upward motion and create a more favourable environment for tropical cyclone development. It is noted that despite the increased RO observation and data coverage, genesis was not predicted for Hurricane Lisa and Hurricane Ian. Further analysis shows that increasing the number of RO profiles and having the data more evenly distributed help improve the pre-genesis environment, with increased specific humidity and relative vorticity. These findings offer guidance for the design of future satellite observing systems: (1) increased RO profile density, beyond what is currently available operationally, is crucial for improving the representation of the pre-genesis environment, especially in data-sparse regions like the tropical North Atlantic Ocean, and (2) homogeneous data distribution minimizes data gaps and improves the accuracy of the observed atmospheric state, by minimizing the sampling errors.

1 Introduction

Tropical cyclones (TCs) in the North Atlantic Ocean pose significant threat to coastal communities through strong winds, storm surge, heavy rainfall, and tornadoes. Accurate prediction of tropical cyclogenesis, the process by which a pre-existing disturbance evolves into a tropical depression, is critical for early warnings, evacuation planning, and risk mitigation. However, forecasting TC genesis remains a major challenge due to the multiscale and nonlinear nature of the processes involved, as well as the scarcity of observations over topical oceans where these systems develop.

One of the primary challenges in forecasting TC genesis stems from the difficulty in detecting and initializing weak, disorganized disturbances. Moist convection plays a central role in this process, yet its episodic and stochastic nature, combined with limited model resolution and sparse environmental moisture observations, makes an accurate prediction challenging

https://doi.org/10.5194/egusphere-2026-2704
Preprint. Discussion started: 27 May 2026

(Wang et al., 2018; Tang et al., 2020; Rajasree et al., 2023). Moreover, the convective organization and vorticity aggregation necessary for genesis are highly sensitive to environmental conditions. Small errors in the thermodynamic or dynamic structure of the model initial condition can result in significant deviation in forecasts, including whether genesis occurs, the timing of intensification, and the storm's subsequent trajectory.

Given the high sensitivity of TC genesis to moisture and vortex structure, improved observations of the thermodynamic environment are essential. The assimilation of satellite-based observations, particularly Global Navigation Satellite System (GNSS) radio occultation (RO), has been shown to enhance representation of lower- and mid-tropospheric moistures, improve the depiction of mid-level vorticity, and support convection organization, thereby creating a more favorable environment for genesis (Liu et al., 2012; Chen et al., 2020; Teng et al., 2022; Yang et al., 2023). Using observing system simulation experiments, Yang et al. (2023) demonstrated that dense GNSS RO observations substantially improved the forecast of Hurricane Gordon's genesis.

Building on these findings, studies in the western North Pacific have demonstrated the critical role of moisture in tropical cyclogenesis under easterly wave environments. Teng et al. (2021) reported a remarkable increase in TC formation detection rates from 7.7 % to 61.5 % after assimilating GNSS RO observations, emphasizing that the probability of genesis strongly depends on the ambient moisture distribution. In the North Atlantic, approximately 60 – 71 % of TCs originate from African easterly waves that propagate westward into the tropical ocean (Landsea, 1993; Russell et al., 2017; Du et al., 2025). The development potential of these waves is modulated by the thermodynamic and oceanic environment, including mid-tropospheric humidity, rain rate, and sea surface temperature (Peng et al., 2012). These factors collectively influence convective aggregation and the amplification of vorticity through latent heat release, as moisture condensation produces diabatic heating and subsequently strengthens the vortex circulation. By providing vertical profiles of temperature and moisture GNSS RO observations can more accurately capture the thermodynamic environment which are favorable for the development of tropical cyclones. Therefore, assimilating dense GNSS RO observations holds promise for improving genesis prediction associated with African easterly waves in the North Atlantic basin.

Motivated by these findings, this study leverages data from the Radio Occultation Modeling Experiment (ROMEX; Anthes et al., 2024), which provides more than three times the number of GNSS RO profiles compared to the operational RO dataset. ROMEX offers an unprecedented opportunity to investigate how the RO data volume and coverage affects tropical cyclogenesis prediction in the North Atlantic. Focusing on selected TCs during the 2022 Atlantic hurricane season, this study aims to assess the impact of enhanced RO sampling on the analyses and prediction of tropical cyclogenesis.

The remainder of the paper is organized as follows. Section 2 describes the datasets and method, including the design of GNSS RO datasets, model configuration, data assimilation experiments, and TC tracking algorithm. Section 3 presents the simulation results of tropical cyclogenesis for selected cases. Sections 4 and 5 examine a representative successful case and one representative failed case, respectively, with particular emphasis on the impact of RO observations. Section 6 summarizes the key findings and implications for future observing system design and operational forecasting.

https://doi.org/10.5194/egusphere-2026-2704
Preprint. Discussion started: 27 May 2026

2 Data and method

2.1 Data

To explore the impact of GNSS RO data coverage on tropical cyclogenesis prediction, three RO datasets, named 8k baseline RO dataset, 14k best distributed RO dataset, and 14k poorest distributed RO dataset, are constructed from the ROMEX data (Anthes et al., 2024) by varying the RO satellite missions. The terms "best" and "poorest" are defined relative to the three datasets used in this study. Figure 1 shows the RO data coverage and amount for each dataset within a 6-hour data assimilation window. As shown in Fig. 1a, 8k baseline RO dataset provides around 8,000 RO soundings globally per day, which includes COSMIC-2, Sentinel-6, MetOp-B/C, PAZ, TanDEM-X, TerraSAR-X, and KOMPSAT-5 missions and is mainly concentrated within the tropical and subtropical regions (~between 40˚N and 40˚S). The largest contributor is the COSMIC-2 mission. Figure 1b shows the data coverage of 14k best distributed RO dataset with around 14,000 RO soundings globally per day, which includes the same RO soundings as in the 8k baseline RO dataset but also two commercial RO satellite missions (e.g., eight Spire satellites and two PlanetiQ satellites). Compared to 8k baseline RO dataset, the 14k best distributed RO dataset not only includes more soundings in the subtropical and tropical regions but also additional soundings in the extratropical region. The increased data volume in the tropical ocean is expected to benefit the tropical cyclogenesis prediction. On the contrary, the 14k poorest distributed RO dataset represents a heterogeneous coverage of RO data (Fig. 1c), which includes MetOp-B/C, GeoOptics, twelve of the Spire satellites, and one of the PlanetiQ satellites. Even though the total amount of soundings is like that of the 14k best distributed RO dataset, the heterogeneous distribution creates a data gap in certain longitude bands. For example, in the North Atlantic Ocean, the RO soundings are only available at 0000 and 1200 UTC daily, which could potentially degrade the tropical cyclogenesis prediction.

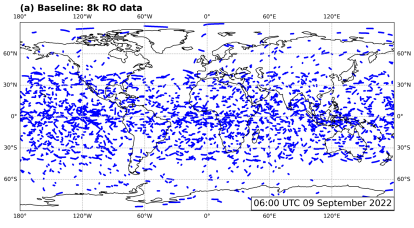

Mission	Number of Profiles	Percentage (%)
COSMIC-2	1490	75.06
KOMPSAT-5	0	0.00
MetOp-B	132	6.65
MetOp-C	121	6.10
PAZ	1	0.05
Sentinel-6	241	12.14
TanDEM-X	0	0.00
TerraSAR-X	0	0.00
Total	1985	100.00

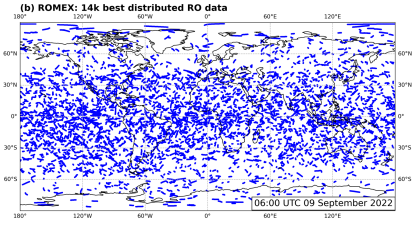

Mission	Number of Profiles	Percentage (%)
COSMIC-2	1490	41.85
KOMPSAT-5	0	0.00
MetOp-B	132	3.71
MetOp-C	121	3.40
PAZ	1	0.03
Sentinel-6	241	6.77
TanDEM-X	0	0.00
TerraSAR-X	0	0.00
PlanetiQ	729	20.48
Spire	846	23.76
Total	3560	100.00

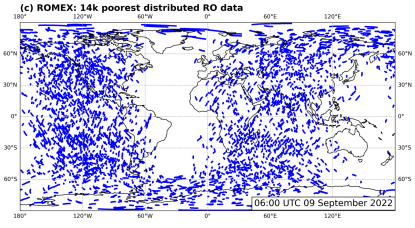

Mission	Number of Profiles	Percentage (%)
GeoOptics	101	2.74
MetOp-B	132	3.58
MetOp-C	121	3.28
PlanetiQ	409	11.10
Spire	2921	79.29
Total	3684	100.00

https://doi.org/10.5194/egusphere-2026-2704
Preprint. Discussion started: 27 May 2026

Figure 1: Global distribution of GNSS RO data and the number of profiles for each satellite mission within a 6-hour window valid at 0600 UTC 9 September 2022 from (a) the 8k baseline RO dataset, (b) the 14k best-distributed RO dataset, and (c) the 14k poorest-distributed RO dataset.

In addition to the GNSS RO data, we also assimilate conventional observation and some infrared and microwave satellite radiance in each DA experiment. The conventional observations are from the NCEP Automated Data Processing (ADP) Global Upper Air and Surface Weather Observations which includes surface observations, radiosondes, aircraft, and satellite-derived winds. The satellite radiance data is from the Advanced Microwave Sounding Unit-A (AMSU-A) on board the NOAA-15/18/19 satellites, the High Resolution Infrared Radiation Sounder (HIRS/4) on board the NOAA-18/19, the Microwave Humidity Sounder (MHS) on board the NOAA-19 and MetOp-B/C, the Advanced Technology Microwave Sounder (ATMS) on board the Suomi National Polar-orbiting Partnership (NPP) satellite, and the Special Sensor Microwave Imager/Sounder (SSMIS) on board the Defense Meteorological Satellite Program (DMSP) F16 satellite.

The NCEP Global Forecast System (GFS) 0.25˚ × 0.25˚ analyses are used as the initial condition for the cold start simulation and as the 6-hourly updated boundary conditions of each DA experiment. The GFS analyses is also used to verify the model analyses and forecasts. The model prediction of tropical cyclogenesis time is verified against the best track data from the National Hurricane Center (NHC), National Oceanic and Atmospheric Administration (NOAA). The observed tropical cyclogenesis time is defined as the time when the tropical depression is first recorded in the best track report.

2.2 Model configuration and experimental design

The overarching goal of this study is to explore the impact of data coverage on the regional tropical cyclogenesis prediction over the North Atlantic Ocean. For each tropical cyclone, three data assimilation experiments, named 8kRO, 14kBestRO, and 14kPoorRO experiments, are performed by assimilating 8k baseline RO dataset, 14k best distributed RO dataset, and 14k poorest distributed RO dataset, respectively (Table 1). Individual DA experiment is conducted using the Weather Research and Forecasting (WRF) Model version 4.6.0 (Skamarock et al., 2019) and the WRF Data Assimilation (WRFDA) system version 4.6.1 (Barker et al., 2012). A single model domain (662 × 386 grid points) with a 15-km horizontal grid spacing covers all genesis cases (Fig. 2a). The 15-km grid spacing is selected based on prior studies (Chen et al., 2020; Teng et al., 2022). Li and Pu (2014) showed limited improvement in cyclogenesis prediction with a higher resolution. The domain uses 52 vertical layers, extending to 20 hPa (~23 km). Key physics parameterizations of this study include: the Goddard microphysics scheme (Tao et al., 1989; Tao et al., 2016), the multi-scale Kain-Fritsch cumulus scheme (Zheng et al., 2016; Glotfelty et al., 2019), the Mellor-Yamada Nakanishi Niino (MYNN) level 3 planetary boundary layer and surface layer schemes (Nakanishi and Niino, 2006, 2009; Olson et al., 2019, 2021), the Rapid Radiative Transfer Model for general circulation models (RRTMG) shortwave and longwave radiation schemes (Iacono et al., 2008), and the Unified Noah land surface model (Tewari et al., 2004).

Table 1: Data assimilation experiments and their corresponding GNSS RO datasets.

https://doi.org/10.5194/egusphere-2026-2704
Preprint. Discussion started: 27 May 2026

Experiment	Assimilated RO Dataset
8kRO	8k baseline RO dataset
14kBestRO	14k best distributed RO dataset
14kPoorRO	14k poorest distributed RO dataset

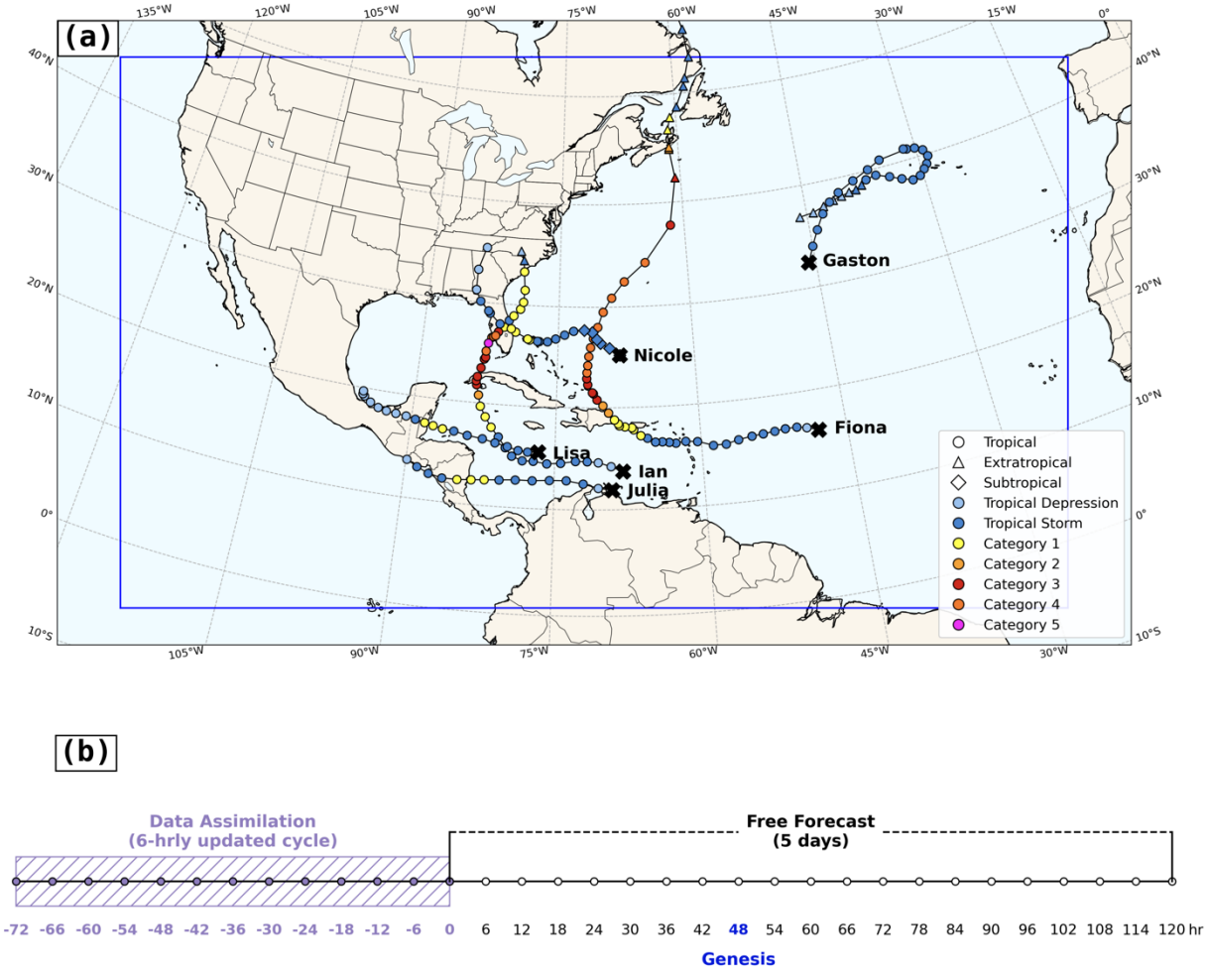

Figure 2: (a) Best track positions of Hurricanes Fiona, Ian, Julia, Lisa, Nicole, and Tropical Storm Gaston. The blue rectangle indicates the WRF model domain. (b) Schematic diagram illustrating the experimental configuration, consisting of a 3-day data assimilation cycling period followed by a 5-day free forecast.

The nonlocal observation operator (Sokolovskiy et al., 2005a, b; Chen et al., 2009) is used to assimilate GNSS RO refractivity data in the WRFDA system. The RO data quality control (QC) in WRFDA includes a background check by computing the background departure, defined as the difference between an observation and its model counterpart. If the background departure

https://doi.org/10.5194/egusphere-2026-2704
Preprint. Discussion started: 27 May 2026

exceeds a predefined threshold, the observation is discarded. This predefined threshold is set to five times the observation error, which is the default value in the WRFDA system.

Our data assimilation strategy follows that of Chen et al. (2020), in which 72-h cycling data assimilation is conducted at 6-h interval from T = -72 h to T = 0 h (Fig. 2b). The start of the forecast (T = 0 h) is 48 hours prior to the actual TC genesis time. The three-dimensional variational (3DVar) method is used for 6-hour cycling data assimilation. After 3-day continuously cycling, a 5-day free forecast is performed. The tropical cyclone (TC) tracking algorithm, discussed in the next section, is used to detect a tropical cyclogenesis.

2.3 TC tracking algorithm

The tropical cyclone (TC) tracking algorithm follows the methods used in Majumdar and Torn (2014) and Hartman et al. (2023). Their methods have been successfully applied to detect TC locations in the North Atlantic Ocean, making them suitable for this study. Several criteria must be met for tropical cyclogenesis. First, a local maximum in the 700-850 hPa layer-averaged circulation is required. The circulation is defined as the average relative vorticity within a 50 km radius of a grid point. For this criterion to be met, the relative vorticity averaged between 700 and 850 hPa must be a local maximum exceeding 4×10^{-5} s^{-1}.

Second, a local maximum in the 200-850 hPa thickness anomaly must be present. The thickness anomaly is defined as the difference between the 200-850 hPa thickness at a given grid point and the domain-averaged thickness. A valid local maximum must exceed 20 m.

Third, a local minimum in mean sea level pressure must be found, with values lower than 1020 hPa. These three extrema should lie within 2° of one another and persist for at least 12 hours (Teng et al., 2022). The first time all these criteria are satisfied is defined as the time of tropical cyclogenesis.

3 Tropical cyclones and their cyclogenesis prediction

To assess the impact of data coverage on regional tropical cyclogenesis prediction over the North Atlantic Ocean, six tropical cyclones (TCs) from the 2022 Hurricane season were selected: Hurricane Fiona, Tropical Storm Gaston, Hurricane Ian, Hurricane Julia, Hurricane Lisa, and Hurricane Nicole (Fig. 2a). Three of these cyclones, Fiona, Ian, and Nicole, made landfall in U.S. territories and caused billion-dollar damages (NOAA, 2025). Julia and Lisa made landfall in Central America, whereas Gaston remained over the open North Atlantic throughout its life cycle. The NHC defined genesis times of these cyclones, ranging from September to November, falling within the ROMEX period (Table 2). Genesis locations are marked as black crosses in Fig. 2a. Fiona formed in the central tropical Atlantic; Gaston developed at a similar longitude but farther north. Ian, Julia, and Lisa all formed within the Caribbean Sea, while Nicole developed much later in the season, near the western edge of the central North Atlantic, close to the Bahama and the U.S. East Coast.

https://doi.org/10.5194/egusphere-2026-2704
Preprint. Discussion started: 27 May 2026

Table 2: Cyclogenesis results for six tropical cyclones. Genesis times are shown relative to the NHC-defined genesis time: a positive value (+) indicates delayed genesis, a negative value (-) indicates early genesis, a cross (×) indicates no genesis, and a triangle (△) signifies that initial genesis occurred but did not persist or intensify into a tropical storm. The probability of detection is also listed for each experiment (see text in Section 3 for definition).

Tropical Cyclone	Observed TC Genesis	8kRO	14kBestRO	14kPoorRO
Fiona	06 UTC 14 Sep	△	+36 hr	×
Gaston	12 UTC 20 Sep	×	△	×
Ian	06 UTC 23 Sep	×	×	×
Julia	00 UTC 07 Oct	-24 hr	+12 hr	+42 hr
Lisa	12 UTC 31 Oct	×	×	×
Nicole	06 UTC 07 Nov	+66 hr	-18 hr	+24 hr
Probability of Detection		16.7 %	33.3 %	16.7 %

Except for Nicole, all selected TCs originated under generally similar environmental conditions. Each cyclone was linked to tropical waves propagating westward from the African coast (Pasch et al., 2023; Pasch, 2023; Bucci et al., 2023, Cangialosi, 2023; Blake, 2023; Beven II and Alaka, 2023). Some disturbances were accompanied by sustained convective activities, while others initially struggled due to unfavorable conditions such as mid-level dry-air intrusions or moderate-to-strong vertical wind shear. As convection became more persistent and better organized, cyclogenesis occurred. In contrast, Nicole experienced a distinctly different cyclogenesis process. It originated from a cutoff low embedded within the mid-latitude westerlies. As the low drifted eastward from the U.S. East Coast over the Atlantic, it transitioned into a tropical cyclone (Bucci et al., 2023) as it interacted with the Intertropical Convergence Zone (ITCZ) under the favorable condition of upper-level divergence.

After establishing the environmental condition for each genesis event, we evaluated how well each DA experiment predicted the timing and occurrence of TC formation. Forecast skill was quantified by the number of successfully detected genesis events using the TC tracking algorithm discussed in Section 2.3. Figure 3 illustrates three candidate disturbances that satisfy all the algorithm criteria: a local maximum in 700-850 hPa circulation (Fig. 3a), a local minimum in mean sea level pressure (Fig. 3b), and a local maximum in 200-850 hPa thickness anomaly (Fig. 3c). Two of the disturbances were also associated with 10-m wind speeds exceeding 25 kt (Fig. 3d). The algorithm was applied hourly to each forecast to determine the first time a TC was identified, defined as the predicted genesis time, and summarized in Table 2. This approach allows direct comparison of the tropical cyclogenesis prediction performance among the different DA experiments.

https://doi.org/10.5194/egusphere-2026-2704
Preprint. Discussion started: 27 May 2026

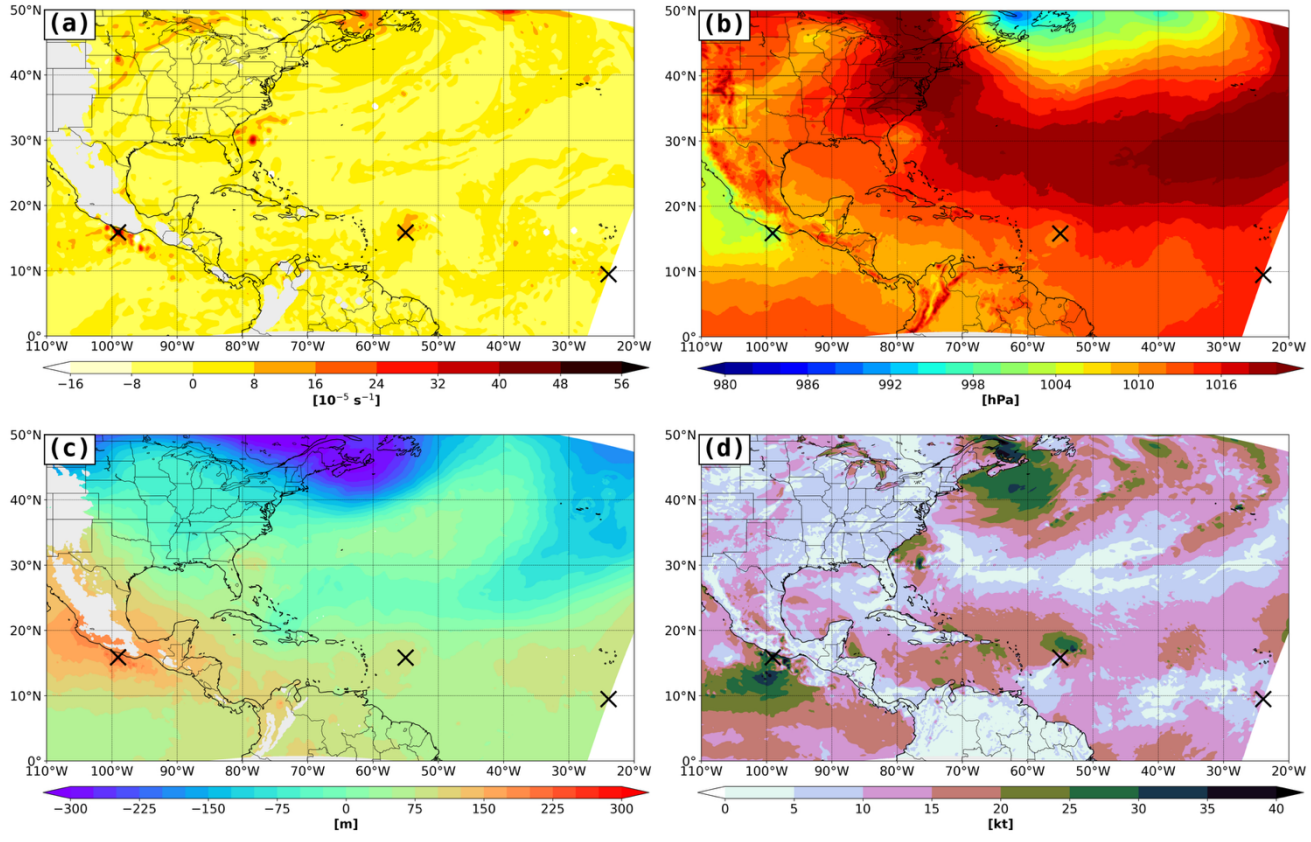

175 **Figure 3: (a) 700-850 hPa layer-averaged circulation (shaded; 10^{-5} s^{-1}), (b) mean sea level pressure (shaded; hPa), (c) 200-850 hPa thickness anomaly (shaded; m), and (d) 10-m wind speed (shaded; kt) from the 14kBestRO experiment at 0000 UTC 16 September 2022. The black cross marks the disturbance that meets all criteria of the TC tracking algorithm.**

The three DA experiments exhibited varying degrees of success in capturing the genesis and its timing relative to the observations (Table 2). In reference to the timing of observed cyclogenesis, a plus sign (+) indicates delayed genesis, a minus
180 sign (–) indicates early genesis, and a cross (×) indicates no genesis. A triangle (△) designates cases where initial genesis was detected but failed to persist or intensify into a tropical storm or hurricane. This is counted as 0.5 hit. For example, 14kBestRO experiment successfully detected the initial genesis of Gaston near the observed time (Fig. 4), but the vortex dissipated in less than 18 hours without further intensification. It should be noted that genesis detection by the tracking algorithm depends on the threshold settings, which may introduce some sensitivity in the determination of the precise genesis time.

https://doi.org/10.5194/egusphere-2026-2704
Preprint. Discussion started: 27 May 2026

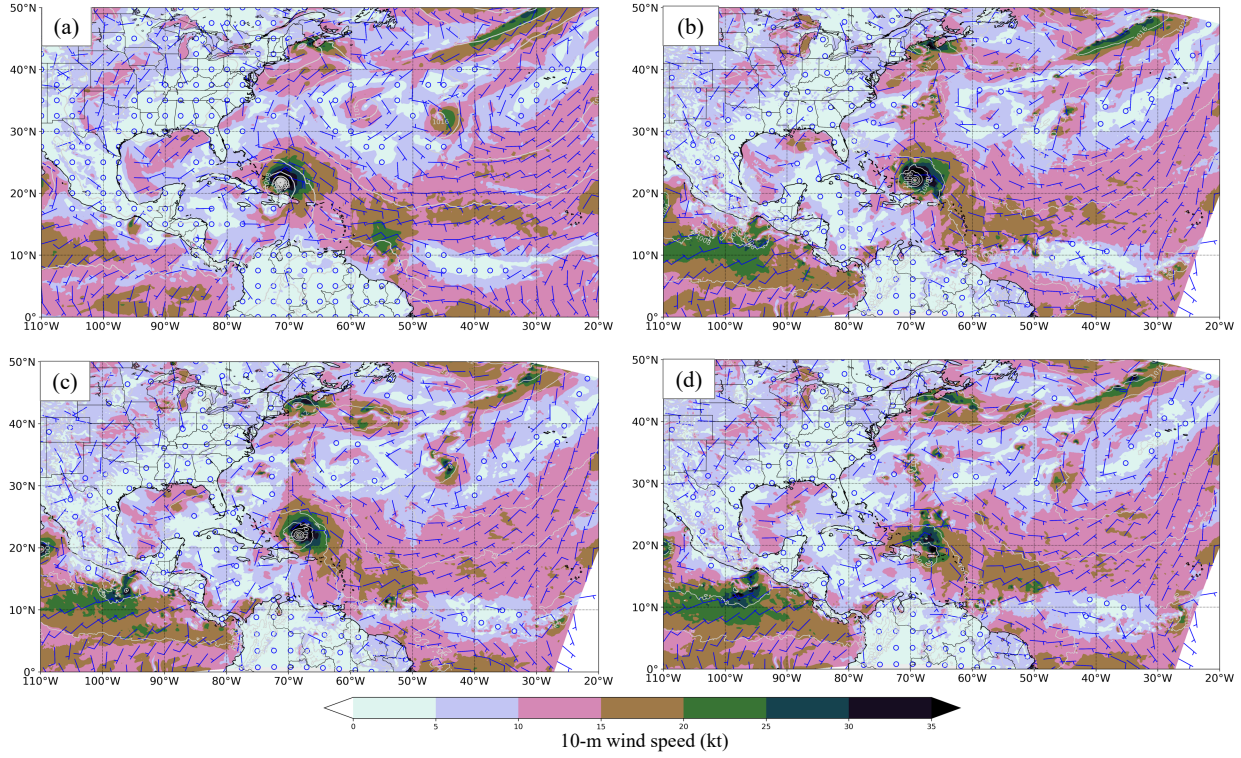

Figure 4: Mean sea level pressure (light gray contours; hPa), 10-m wind speed (shaded; kt), and 10-m wind barbs (kt) valid at 1200 UTC 20 September 2022 from (a) the NCEP GFS analysis and (b – d) the 48-hour forecasts from the (b) 8kRO, (c) 14kBestRO, and (d) 14kPoorRO experiments. Tropical Storm Gaston is located at (32.5° N, 45.8° W) in panel (a).

Overall, the 8kRO experiment captured 2.5 out of 6 TC genesis events, including Nicole, Julia, and the initial genesis of Fiona. The 14kPoorRO experiment predicted 2 out of 6 events, capturing Nicole and Julia. The 14kBestRO experiment predicted 3.5 out of 6 genesis events, including Fiona, Nicole, Julia, and the initial genesis of Gaston. Following Halperin et al. (2013) and Chen et al. (2020), a successful prediction (i.e., a hit) is defined as one in which the model-predicted genesis time falls within ± 24 hours of the observed genesis time. Among the three DA experiments, 14kBestRO showed the highest probability of detection and the closest agreement with the observed genesis times (Table 2).

The improved performance of 14kBestRO likely results from its greater number of GNSS RO profiles assimilated in the troposphere at each DA cycle (Figs. 5a, 5d) and their more homogeneous spatial distribution (Fig. 6b). As shown in Fig. 6, 14kBestRO provided best profile coverage over the North Atlantic compared with the other datasets. Although the 14kPoorRO dataset contains a similar total number of profiles globally, its coverage in the tropical North Atlantic (Fig. 6c) is sparse relative to the other two datasets (Figs. 6a-b). The reduced sampling of the pre-genesis environment likely contributed to its lower forecast skill.

https://doi.org/10.5194/egusphere-2026-2704
Preprint. Discussion started: 27 May 2026

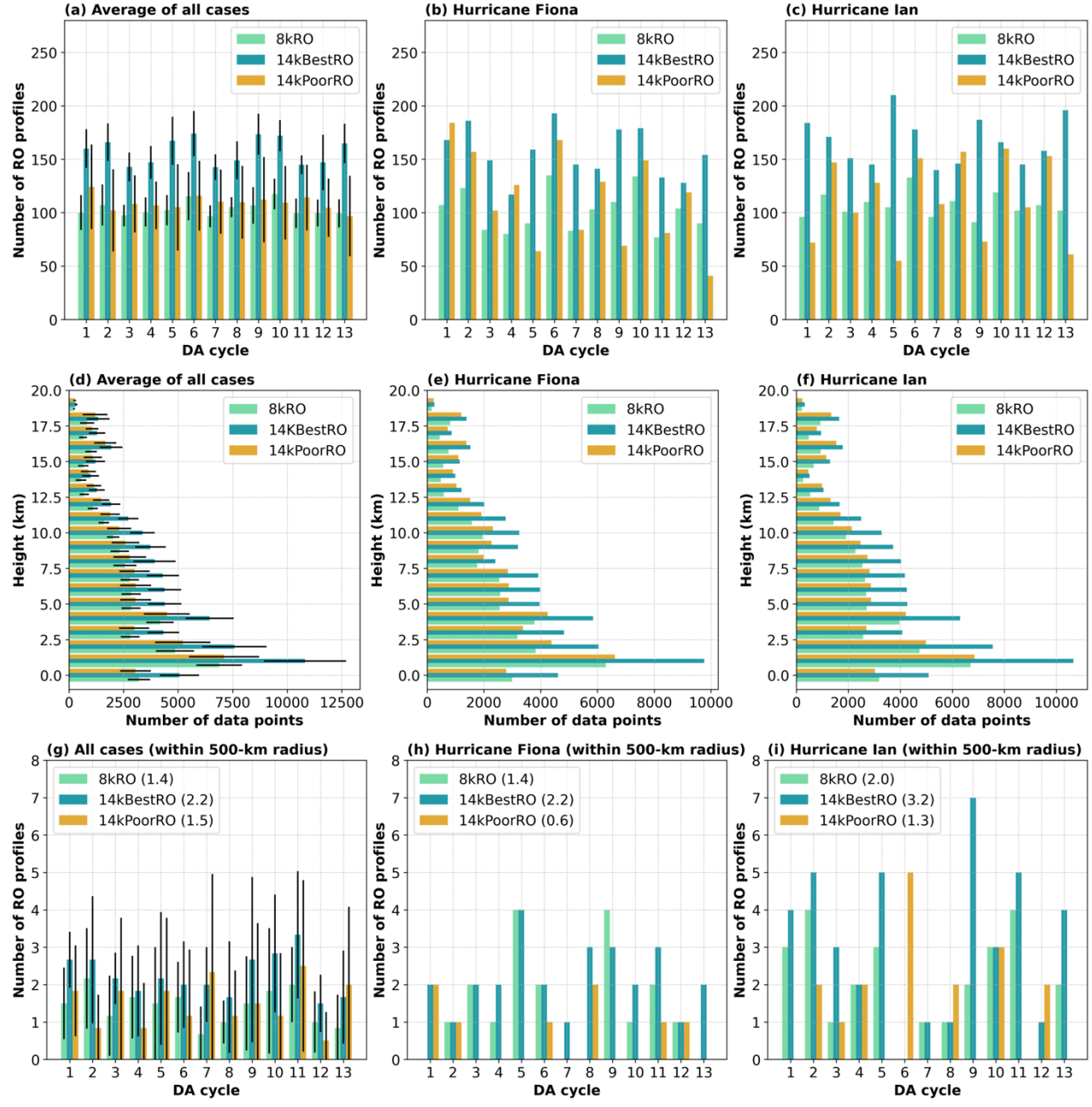

Figure 5: (a-c) Number of assimilated RO profiles at each DA cycle, (d-f) number of assimilated RO data points at each height throughout the DA period, and (g-i) number of assimilated RO profiles within 500 km radius of vortex center at each DA cycle for the 8kRO (cyan), 14kBestRO (blue), and 14kPoorRO (orange) experiments for (a) the average over all selected cases, (b) Hurricane Fiona, and (c) Hurricane Ian. The black vertical/horizontal line in (a), (d), and (e) denotes the standard deviation of the number of profiles.

https://doi.org/10.5194/egusphere-2026-2704
Preprint. Discussion started: 27 May 2026

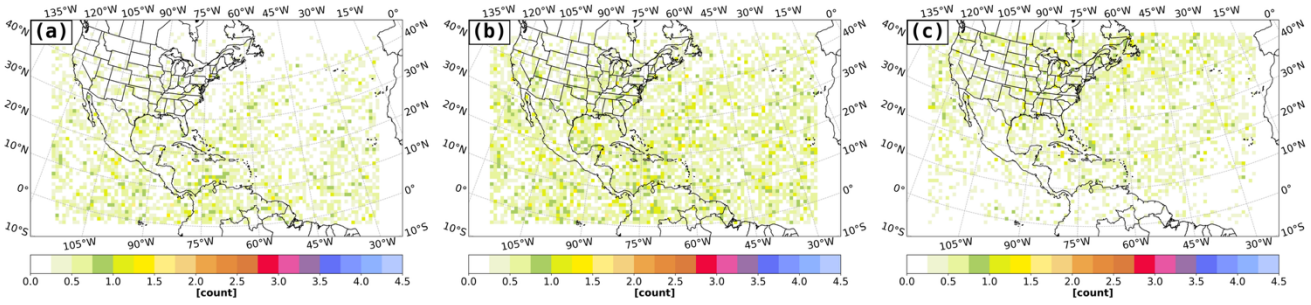

Figure 6: Spatial distribution of total number of assimilated GNSS RO profiles (shaded) during the DA period at each 7-by-7 grid points (approximately 105 km-by-105 km grid size) within the model domain average over all TC cases. Data are shown for (a) the 8kRO dataset, (b) the 14kBestRO dataset, and (c) the 14kPoorRO dataset.

To further evaluate the forecast impact of the RO datasets on the large-scale environment, we computed the normalized root-mean-square error (RMSE) difference relative to the 8kRO experiment as

$$\Delta RMSE_x = \frac{RMSE_{x,DA} - RMSE_{x,8kRO}}{RMSE_{x,8kRO}} \times 100\%$$

where x denotes a forecast variable (e.g., geopotential height, temperature, specific humidity, or horizontal wind components), and "DA" refers to either the 14kBestRO or 14kPoorRO experiment. RMSEs were computed against the GFS analysis at each model layer over the model domain. A negative $\Delta RMSE_x$ indicates an improvement relative to 8kRO, whereas a positive value denotes degradation.

https://doi.org/10.5194/egusphere-2026-2704
Preprint. Discussion started: 27 May 2026

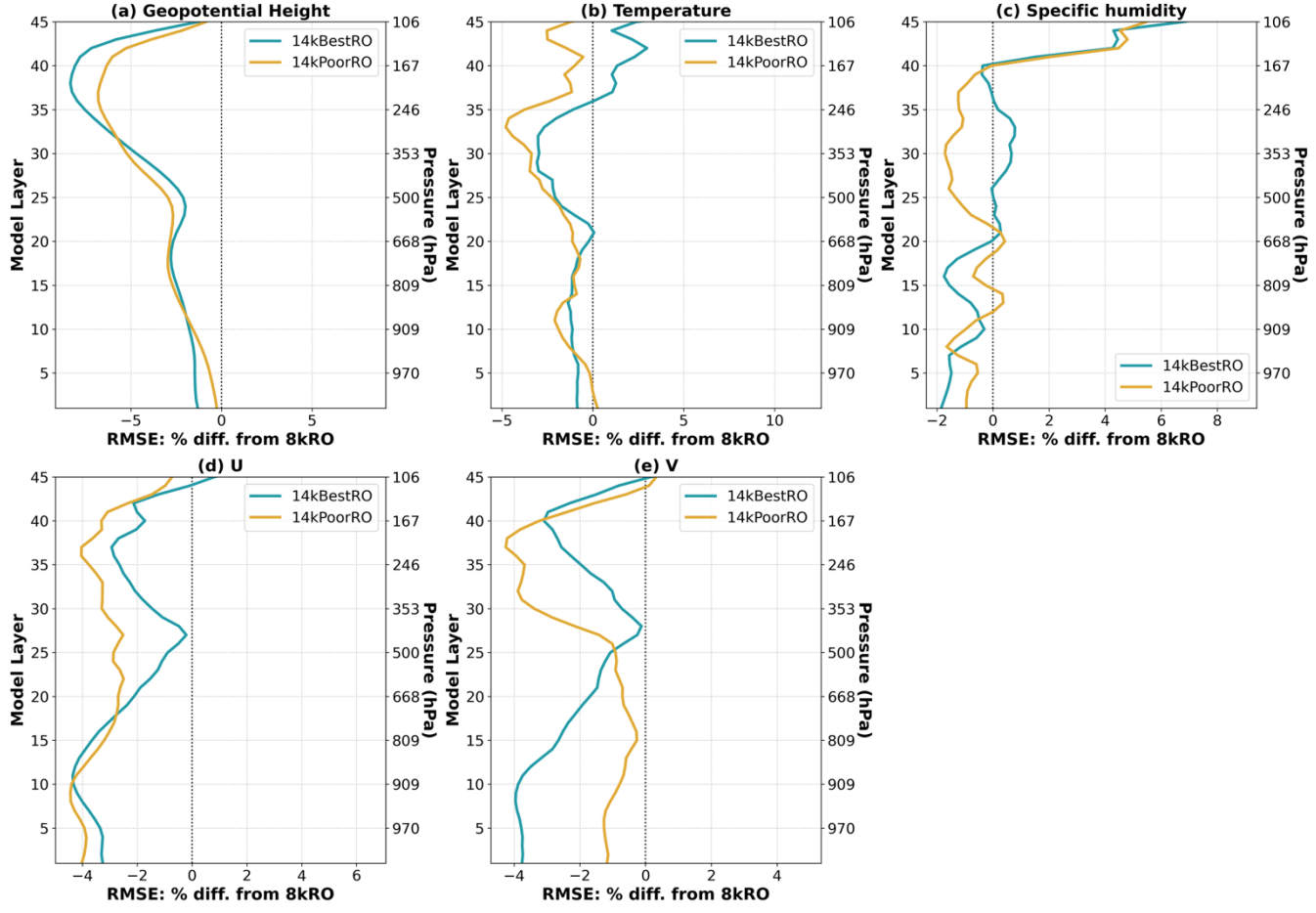

Figure 7: Vertical profiles of ΔRMSE (%) from the 8kRO experiment for (a) geopotential height, (b) temperature, (c) specific humidity, (d) zonal wind (u), and (d) meridional wind (v), comparing the 14kBestRO (blue) and 14kPoorRO (orange) experiments. The left (right) y-axis indicates the model layer (pressure in hPa). Each profile represents the mean ΔRMSE averaged over the forecast period and across six selected TC cases.

Figure 7 shows the mean ΔRMSE profiles averaged over the six tropical cyclone cases. Both 14kBestRO and 14kPoorRO generally show forecast improvements across most variables and vertical layers, with the largest improvement in the v-wind component below model layer 20 (~668 hPa) in 14kBestRO (Fig. 7e). However, above this level, the 14kPoorRO experiment shows larger reductions in RMSE across nearly all variables, including temperature and specific humidity (Figs. 7b-c). This is likely related to the significantly larger number of RO data over high latitudes for 14kPoorRO, where strong upper-level jets are located. These results show that the assimilation of increased RO observations reduced the overall model errors.

The larger ΔRMSE reductions in 14kPoorRO reflect improved forecast of large-scale circulations in higher latitudes (because of increased RO observations in these latitudes). However, such improvement (in high latitudes) does not directly translate to improved prediction of tropical cyclogenesis. Previous studies (i.e., Chen et al 2020) showed that having observations at the right location and right time is critical for RO to have an impact on tropical cyclogenesis. Given the fact that 14kPoorRO has

https://doi.org/10.5194/egusphere-2026-2704
Preprint. Discussion started: 27 May 2026

uneven distribution (both in time and space) over the tropics, it is not surprising that its performance on tropical cyclogenesis prediction is the lowest among the three experiments.

While domain-averaged metrics provide a general assessment of forecast skill, they may mask regional differences critical for TC development. The localized improvements in 14kBestRO (as shown in Fig. 4) highlight the importance of examining model variables that are sensitive to tropical cyclogenesis, rather than relying solely on domain-wide statistics. The following section presents a detailed comparison of relative humidity and vorticity fields near storm centers to further illustrate these regional improvements.

As noted earlier, the genesis of two TCs was not predicted by any experiment. Possible contributing factors include unfavorable environmental conditions for development, model configuration limitations (e.g., DA method, initial/boundary conditions), and sparse observations in key regions. It would still be interesting to examine the impact of increased RO data coverage even though the model failed to capture the genesis. This will be discussed in Section 5. In the next section, we examine one successful case in detail to identify the factors that contributed to its development or lack thereof in the WRF simulation.

4 A successful case – Hurricane Fiona

According to the NHC report (Pasch et al., 2023), Hurricane Fiona originated from an easterly wave that moved off the West African coast. On 10 – 11 September, the disturbance experienced a dry-air intrusion that suppressed convective activity. As the system propagated westward across the tropical Atlantic, deep convection became more organized and persistent. By 0600 UTC 14 September, a well-defined low-level circulation had formed, marking the onset of tropical cyclogenesis. During the first three days (14 – 16 September), Fiona experienced moderate-to-strong westerly vertical wind shear, with its low-level circulation center displaced west of the deep convection. This structure is clearly visible in the GOES-16 satellite imagery (see CSU/CIRA & NOAA archive: https://satlib.cira.colostate.edu/event/hurricane-fiona/).

As discussed in Section 3, denser and more homogeneous data coverage over the tropical North Atlantic contributed to the improved performance of the 14kBestRO experiment. To better understand the physical mechanisms behind this improvement, we examine the evolution of Fiona's dynamic and thermodynamic structure within 10° radius of Fiona.

4.1 Impact of data distribution on Fiona's formation

The increased data coverage in 14kBestRO appears particularly beneficial for predicting Fiona's genesis because of the higher number of assimilated GNSS RO profiles (Figs. 5b and 5e) and a more frequent temporal sampling over the central tropical North Atlantic (Fig. 6b). According to Pasch et al., 2023, the NHC noted that the timing and location of Fiona's genesis were poorly predicted by global models due to errors in representing pre-Fiona disturbance. Assimilating more homogeneously distributed RO profiles may help mitigate such issues by improving analyses of the thermodynamic and dynamic environment.

https://doi.org/10.5194/egusphere-2026-2704
Preprint. Discussion started: 27 May 2026

Within a 500-km radius of the pre-Fiona vortex, 14kBestRO assimilated more profiles than the other two experiments (Fig. 5h), underscoring the importance of near-vortex observations for tropical cyclogenesis prediction (Chen et al., 2020). The vortex center at each analysis or forecast time is defined as the 700 – 850 hPa layer-averaged circulation maximum.

https://doi.org/10.5194/egusphere-2026-2704
Preprint. Discussion started: 27 May 2026

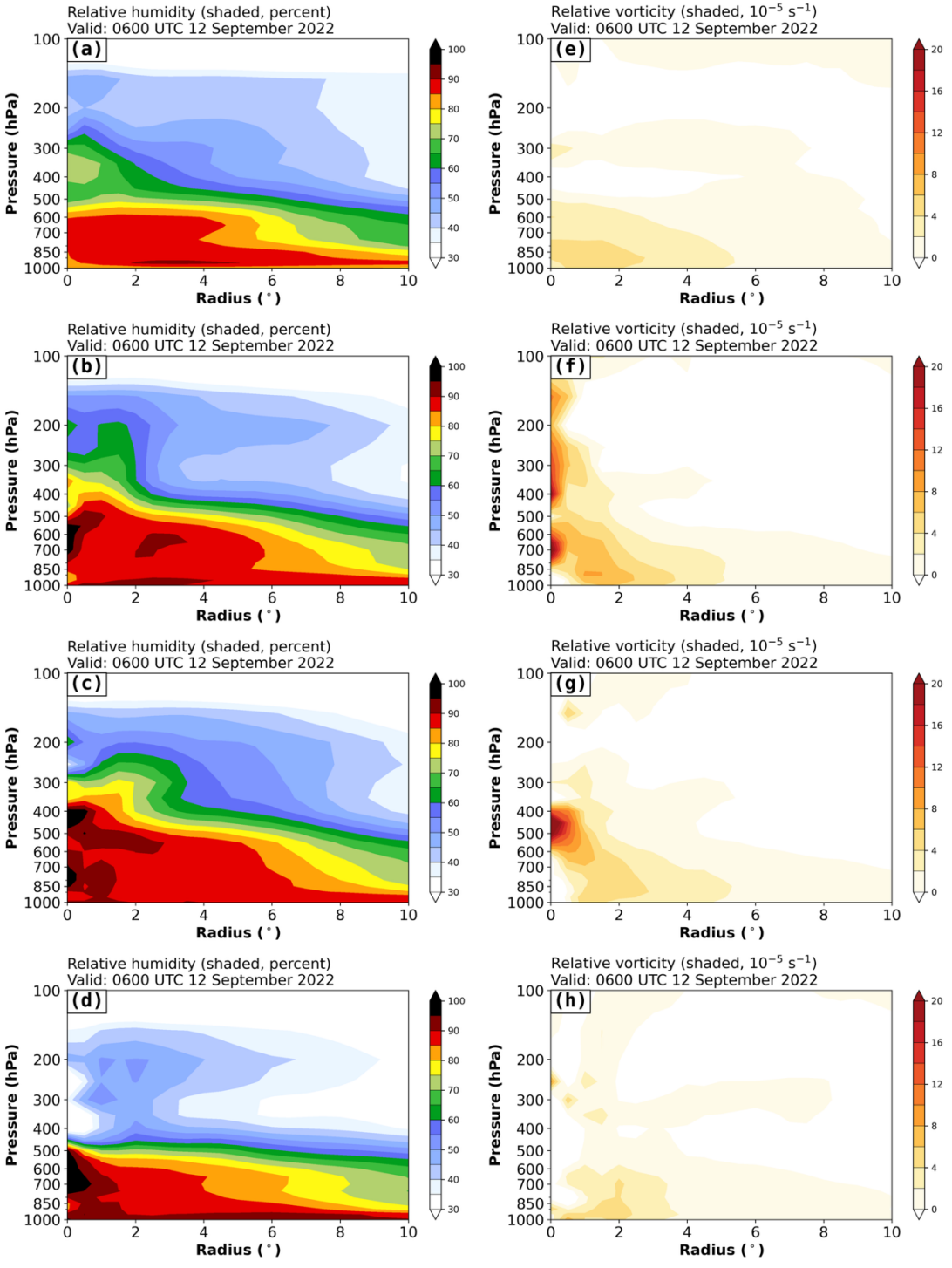

265

https://doi.org/10.5194/egusphere-2026-2704
Preprint. Discussion started: 27 May 2026

Figure 8: Radius-pressure cross-sections of (left column) relative humidity (%) and (right column) relative vorticity (10^{-5} s^{-1}) for (a, e) the GFS analysis, (b, f) 8kRO, (c, g) 14kBestRO, and (d, h) 14kPoorRO experiments at 0600 UTC 12 September 2022. The vortex center is defined at radius = 0˚, and both variables are azimuthally averaged within a 0˚ to 10˚ radius from the vortex center.

Figures 8a-d (8e-f) show the radius-height cross-sections of relative humidity (relative vorticity) averaged around the vortex center for the GFS analysis and the three DA experiments at 0600 UTC 12 September 2022 (i.e., the initial time of the free forecast). In the GFS analysis and the 8kRO and 14kBestRO experiments, a moist layer with relative humidity exceeding 60 % extends up to 200 – 300 hPa within a 2˚ radius of the vortex center (Figs. 8a-c). In contrast, the 14kPoorRO experiment shows a shallower moist layer extending only to about 450 hPa (Fig. 8d). Regarding the vorticity structure, the GFS analysis exhibits a low-level maximum below 800 hPa (Fig. 8e). While the maximum vorticity occurs slightly higher in the 8kRO and 14kBestRO experiments (Figs. 8f-g), both maintain comparable strength to the GFS analysis in the lower levels within a 2˚ radius. The 14kPoorRO experiment, however, displays substantially weaker and shallower low-level vorticity (Fig. 8h), suggesting weaker dynamical support for cyclogenesis at the initial forecast time. It should be that these three DA experiments started with the same GFS analysis at t = -72 h (the start of data assimilation). Through cycling assimilation of RO data with different data volume and coverage, the final analysis (at t = 0 h) exhibits significant differences in both vorticity and humidity structure. These differences highlight the advantage of denser RO sampling in the tropical North Atlantic, particularly for representing the pre-genesis environment.

https://doi.org/10.5194/egusphere-2026-2704
Preprint. Discussion started: 27 May 2026

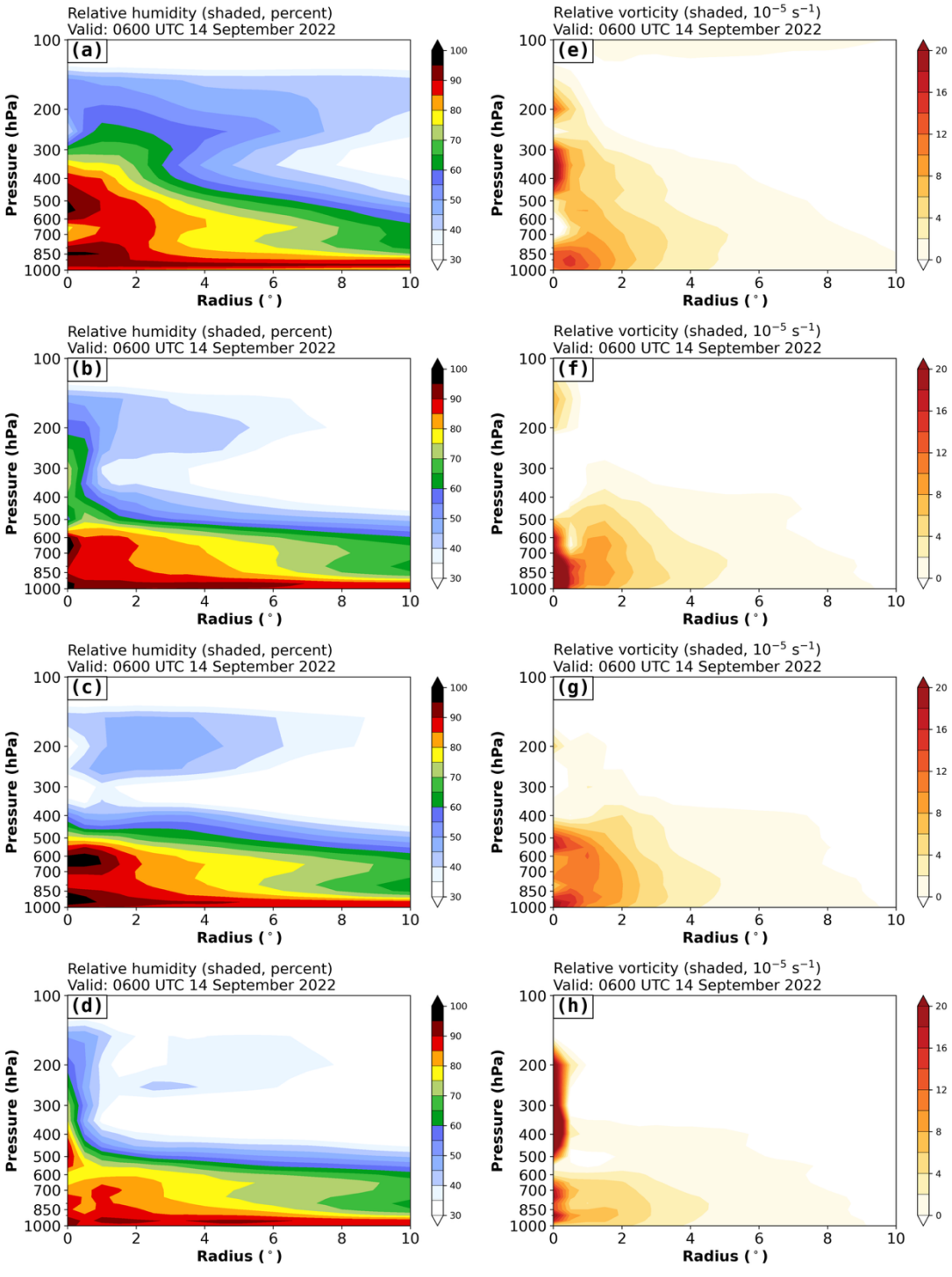

Figure 9: Same as Fig. 8, but at 0600 UTC 14 September 2022.

https://doi.org/10.5194/egusphere-2026-2704
Preprint. Discussion started: 27 May 2026

Figure 9 depict the same model variables 48 hours later, at 0600 UTC 14 September 2022, when Fiona's observed genesis occurred. The GFS analysis shows two relative humidity maxima: one below 800 hPa and another between 450 and 600 hPa (Fig. 9a). A similar two-layer structure appears in the DA experiments, with the strongest and broadest moistening in 14kBestRO (Figs. 9b-d). The 14kPoorRO experiment is considerably dryer near the vortex center (Fig. 9d), indicating a less favorable thermodynamic environment for genesis. Concurrently, the GFS analysis exhibits the development of a deep, vertically aligned vortex within a 2˚ radius (Fig. 9e), exhibiting a dynamically and thermodynamically environment favorable for cyclogenesis. The 8kRO and 14kBestRO experiments also develop vertically aligned mid- to low-level vortices (Figs. 9f-g) within a 2˚ radius. In contrast, the very narrow vorticity structure of 14kPoorRO is very different from that of GFS (Fig. 9h) and the other two DA experiments. This alignment between high moisture and high vorticity is crucial for cyclogenesis, consistent with the results of Teng et al. (2021), who emphasized the importance of sufficient midlevel moisture in easterly wave environments.

4.2 Evolution of storm-scale thermodynamic structure

To further examine the evolution of thermodynamic environment leading to Fiona's genesis, we analyzed the time-height evolution of relative humidity and relative vorticity, averaged within 500 km of the vortex center, from the beginning of the DA period (t = -72 h) to the observed genesis (t = 48 h). Figures 10a – b compare the GFS analysis and the 14kBestRO experiment. In the GFS analysis, a midlevel vortex centered at 700 hPa (relative vorticity $\geq 2 \times 10^{-5}$ s^{-1}) is evident between t = -72 h and -48 h (Fig. 10a). This vortex weakened temporarily as dry air intruded between 200 - 450 hPa starting at t = -60 h but subsequently recovered. By t = -12 h, a low-level vortex began to intensify, together with increased relative humidity, culminating a favorable environment for tropical cyclogenesis. The 14kBestRO experiment reproduces a similar evolution (Fig. 10b), although the dry-air intrusion and subsequent low-level vortex development occur later than in the GFS analysis. Additionally, 14kBestRO exhibits weaker relative vorticity below 400 hPa during the DA period and lower upper-tropospheric relative humidity (200 – 400 hPa) between t = 24 h and 48 h (Fig. 10c), which explain its delayed genesis compared with observations.

https://doi.org/10.5194/egusphere-2026-2704
Preprint. Discussion started: 27 May 2026

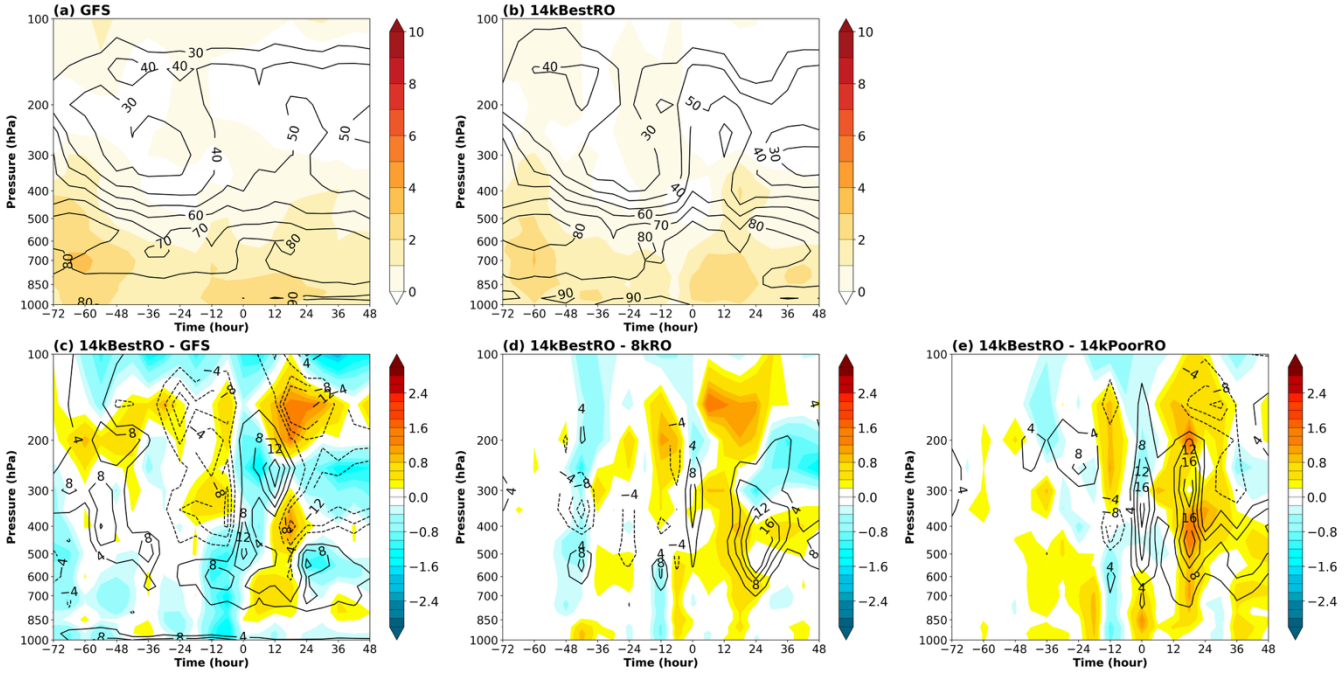

Figure 10: Time-pressure cross-sections of relative humidity (black contours; %) and relative vorticity (shaded; 10^{-5} s^{-1}) for (a) the GFS analysis, (b) the 14kBestRO experiment, and the differences between (c) 14kBestRO and GFS, (d) 14kBestRO and 8kRO, and (e) 14kBestRO and 14kPoorRO. The x-axis indicates time relative to the final data assimilation analysis at t = 0 h. Both variables are azimuthally averaged within a 500-km radius of the vortex center for Hurricane Fiona.

Figures 10d – e show the differences in relative humidity and relative vorticity between the 14kBestRO experiment and the other two experiments (8kRO and 14kPoorRO), averaged within the same radius. The differences are small between t = -72 h and -48 h but become pronounced after t = -48 h. The 14kBestRO exhibits higher relative humidity between 200 – 700 hPa and stronger relative vorticity throughout the troposphere compared with both 8kRO and 14kPoorRO, with the largest difference relative to 14kPoorRO (Fig. 10e). This pattern clearly illustrates the impact of improved RO data coverage (Figs. 5 – 6) over the genesis region. Although the total number of RO profiles globally is comparable, gaps in tropical longitudinal bands in 14kPoorRO reduces its refresh rate and degrade its ability to resolve rapidly evolving storm-scale thermodynamic and dynamic structures.

Overall, the denser and more homogeneous RO sampling in 14kBestRO leads to a more accurate depiction of Fiona's thermodynamic evolution, including stronger mid- to low-level moisture and enhanced cyclonic vorticity near the developing center. The coupling between increased moisture and cyclonic vorticity provides a favorable condition for cyclogenesis and its subsequent intensification, with these improvements extending into the forecast period (t = 0-48 h).

https://doi.org/10.5194/egusphere-2026-2704
Preprint. Discussion started: 27 May 2026

5 A failed case – Genesis Predictability of Hurricane Ian

Hurricane Ian originated from a tropical easterly wave that propagated westward from the coast of West Africa. As the disturbance entered the Caribbean Sea between 21 and 23 September, it encountered moderate-to-strong vertical wind shear associated with the upper-level outflow from Hurricane Fiona to the north. The GFS analysis at 0000 UTC 21 September (t = -6 h) indicates a pronounced dry-air intrusion within a 500-km radius of the disturbance center between 100 and 850hPa (Fig. 11a). At this time, relative vorticity near the vortex center began to strengthen and extend upward to 200 hPa. Approximately 6 hours later, the relative humidity in the lower troposphere increased, providing a favorable environment for Ian's cyclogenesis.

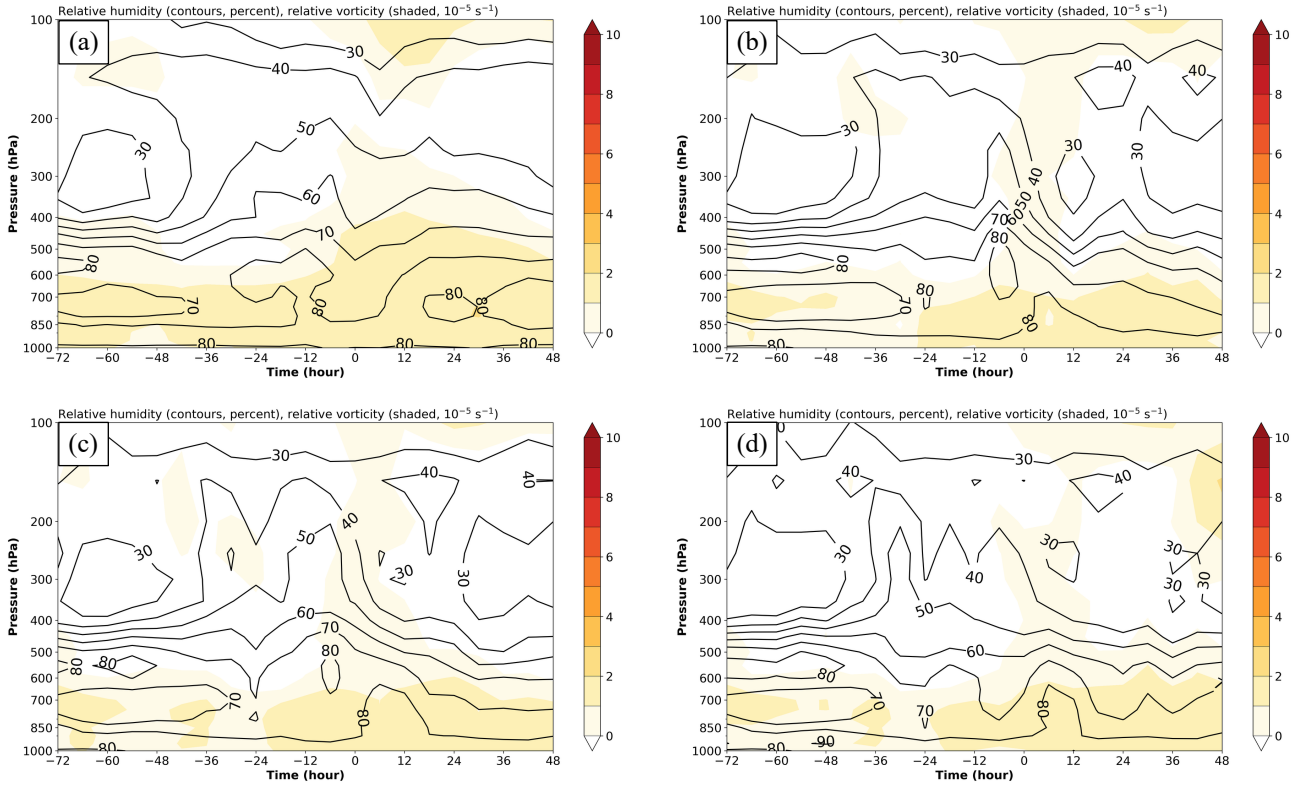

Figure 11: Same as Fig. 10a, but for Hurricane Ian at the corresponding analysis time, showing results from (a) the GFS analysis, (b) 8kRO, (c) 14kBestRO, and (d) 14kPoorRO experiments.

In contrast, none of the three DA experiments reproduced the observed increase in relative humidity or the intensification of vorticity and its upward extension (Fig. 11b-d). The persistent dry-air intrusion in the vicinity of the vortex center likely suppressed convective development, slowing the intensification of the developing vortex.

Although none of the DA experiments successfully predicted Ian's genesis, modest improvements of the pre-genesis environment were evident with the 14kBestRO experiment, which provided denser and more uniform coverage over the tropics (Fig. 6b). The 14kBestRO experiment produced higher 850-hPa relative vorticity and enhanced mid-level (400-700 hPa)

https://doi.org/10.5194/egusphere-2026-2704
Preprint. Discussion started: 27 May 2026

340 relative humidity near the observed genesis location compared to the other two experiments (Figs. 12 and 13). However, the modest moisture increase was insufficient to counteract the ventilation effects of vertical wind shear. This suggests that the model analyses with the assimilation of 14kBestRO dataset is suboptimal, and deserves a closer look.

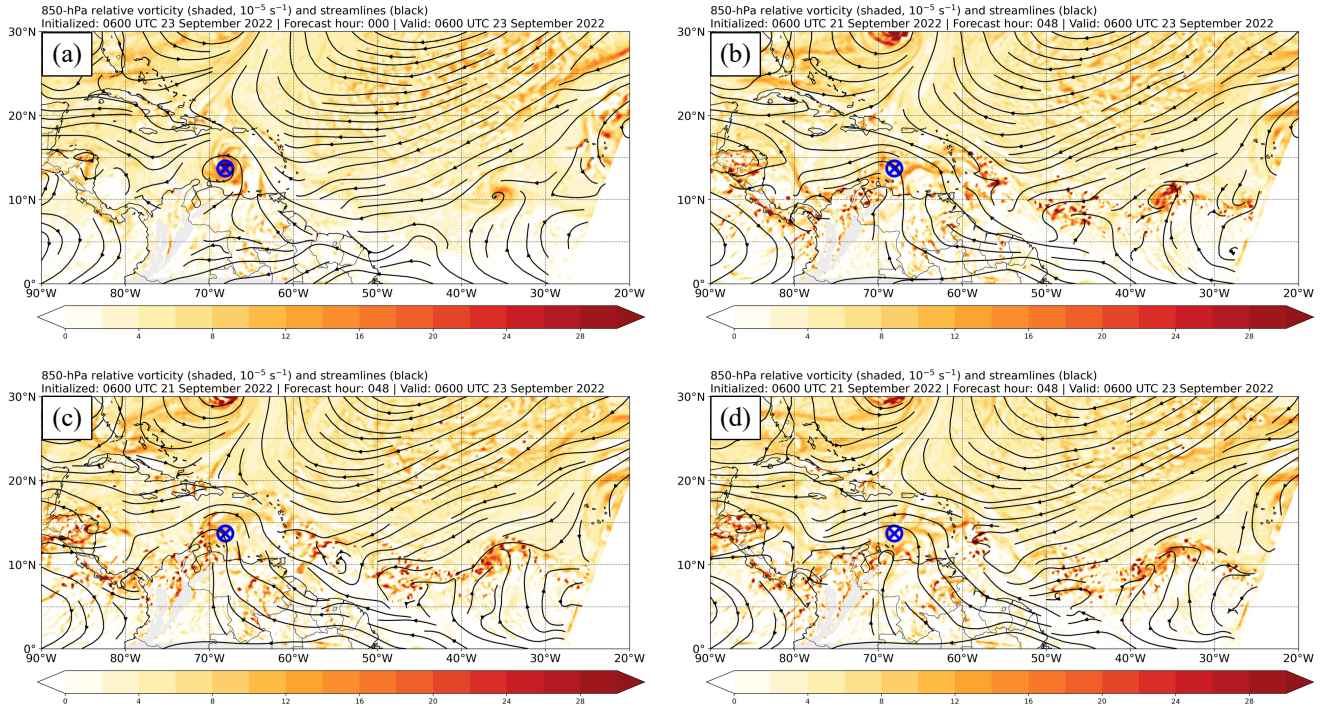

Figure 12: 850-hPa relative vorticity (shaded; 10^{-5} s^{-1}) and streamlines (black) from (a) the GFS analysis, (b) 8kRO, (c) 14kBestRO, and (d) 14kPoorRO experiments at 0600 UTC 23 September 2022, corresponding to the observed genesis time of Hurricane Ian. The
345 **blue cross-within-circle marks the observed genesis location.**

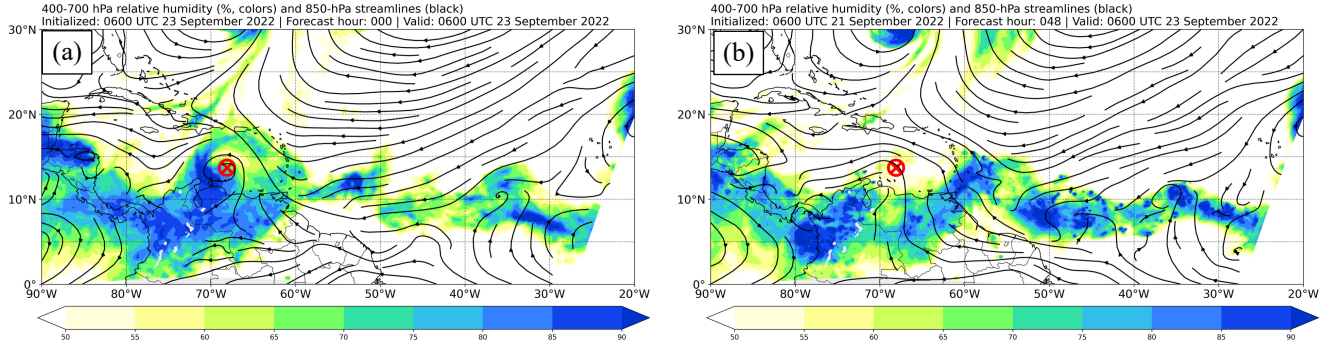

https://doi.org/10.5194/egusphere-2026-2704
Preprint. Discussion started: 27 May 2026

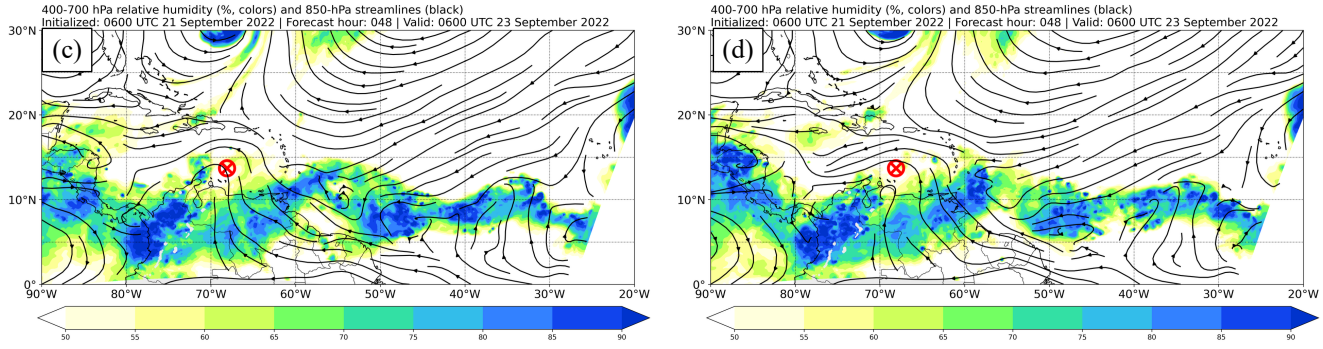

Figure 13: 400-700 hPa relative humidity (shaded; %) and 850-hPa streamlines (black) from (a) the GFS analysis, (b) 8kRO, (c) 14kBestRO, and (d) 14kPoorRO experiments at 0600 UTC 23 September 2022, corresponding to the observed genesis time of Hurricane Ian. The red cross-within-circle marks the observed genesis location.

To further investigate the predictability of Ian's genesis, a series of WRF simulations were initialized from the GFS analyses at 120 (t = -72h), 96, 72, and 48 (t = 0h) hours prior to the observed genesis time (0600 UTC 23 September 2022). Among these simulations, only the 48-h lead-time simulation, hereafter the init_GFS experiment (Table 3), successfully reproduced Ian's genesis (Fig. 14). Clearly, the GFS analysis at t = 0h possesses important signatures in dynamic and thermodynamic fields that were not captured by the three DA experiments. While 14kBestRO performs better than the other two DA experiments, the improvements are not sufficient to produce tropical genesis. This motivated a set of sensitivity experiments to examine factors critical for a successful prediction of Ian's genesis.

Table 3: Sensitivity experiments and their corresponding moisture field.

Experiment	Source of moisture field	Source of other fields
init_GFS	GFS analysis	GFS analysis
GFS_q14kBestRO	14kBestRO final analysis	GFS analysis
14kBestRO_qGFS	GFS analysis	14kBestRO final analysis

https://doi.org/10.5194/egusphere-2026-2704
Preprint. Discussion started: 27 May 2026

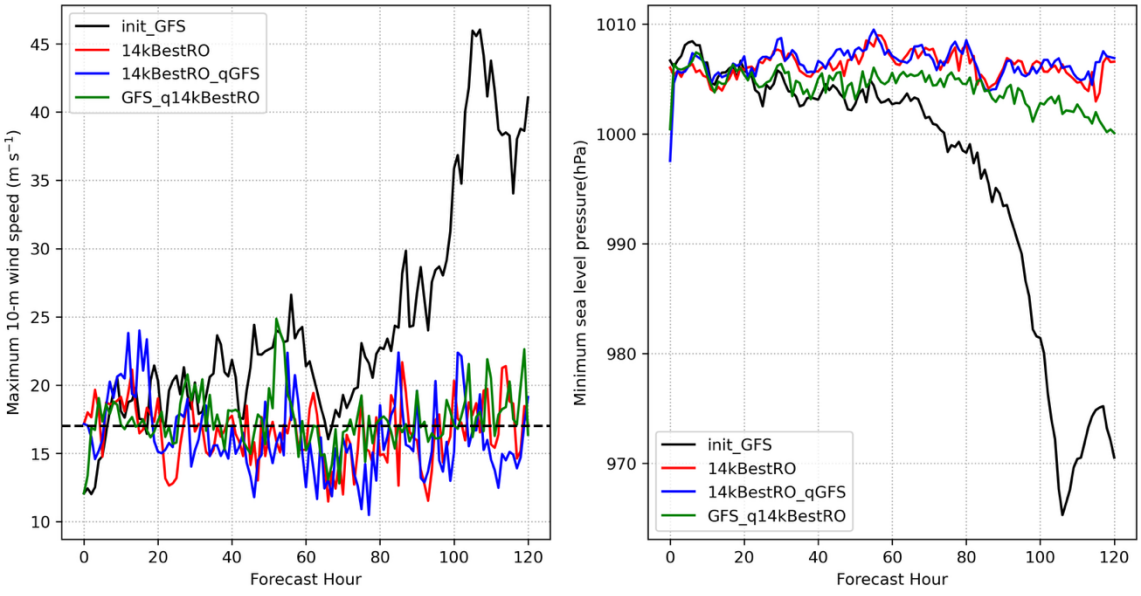

Figure 14: (left) Maximum 10-m wind speed (m s^{-1}) near the low-pressure system and (right) the corresponding minimum sea level pressure for init_GFS (black), 14kBestRO (red), 14kBestRO_qGFS (blue), and GFS_q14kBestRO (green) experiments over the forecast period (t= 0 h to t = 120 h). The black dashed horizontal line on the left panel marks the wind speed of 17 m s^{-1} which is the least surface wind speed for a tropical storm.

Previous studies (e.g., Teng et al., 2021) have shown that moisture plays a key role in tropical cyclogenesis under easterly wave environments. In the North Atlantic, African easterly waves frequently act as precursor disturbances for tropical cyclogenesis by providing low-level cyclonic vorticity; however, whether these disturbances develop into tropical cyclones is strongly influenced by environmental moisture and other thermodynamic and dynamical factors (e.g., Dunkerton et al., 2009; Peng et al., 2012). To further investigate the roles of moisture and dynamical structure in Hurricane Ian's genesis, we conducted two sensitivity experiments: GFS_q14kBestRO and 14kBestRO_qGFS (Table 3).

In the GFS_q14kBestRO experiment, the water vapor mixing ratio in the GFS analysis was replaced with that from the final 14kBest RO analysis. Conversely, in the 14kBestRO_qGFS experiment, the moisture field in the final 14kBest RO analysis was replaced with that from the GFS analysis prior to a 120-h free forecast.

https://doi.org/10.5194/egusphere-2026-2704
Preprint. Discussion started: 27 May 2026

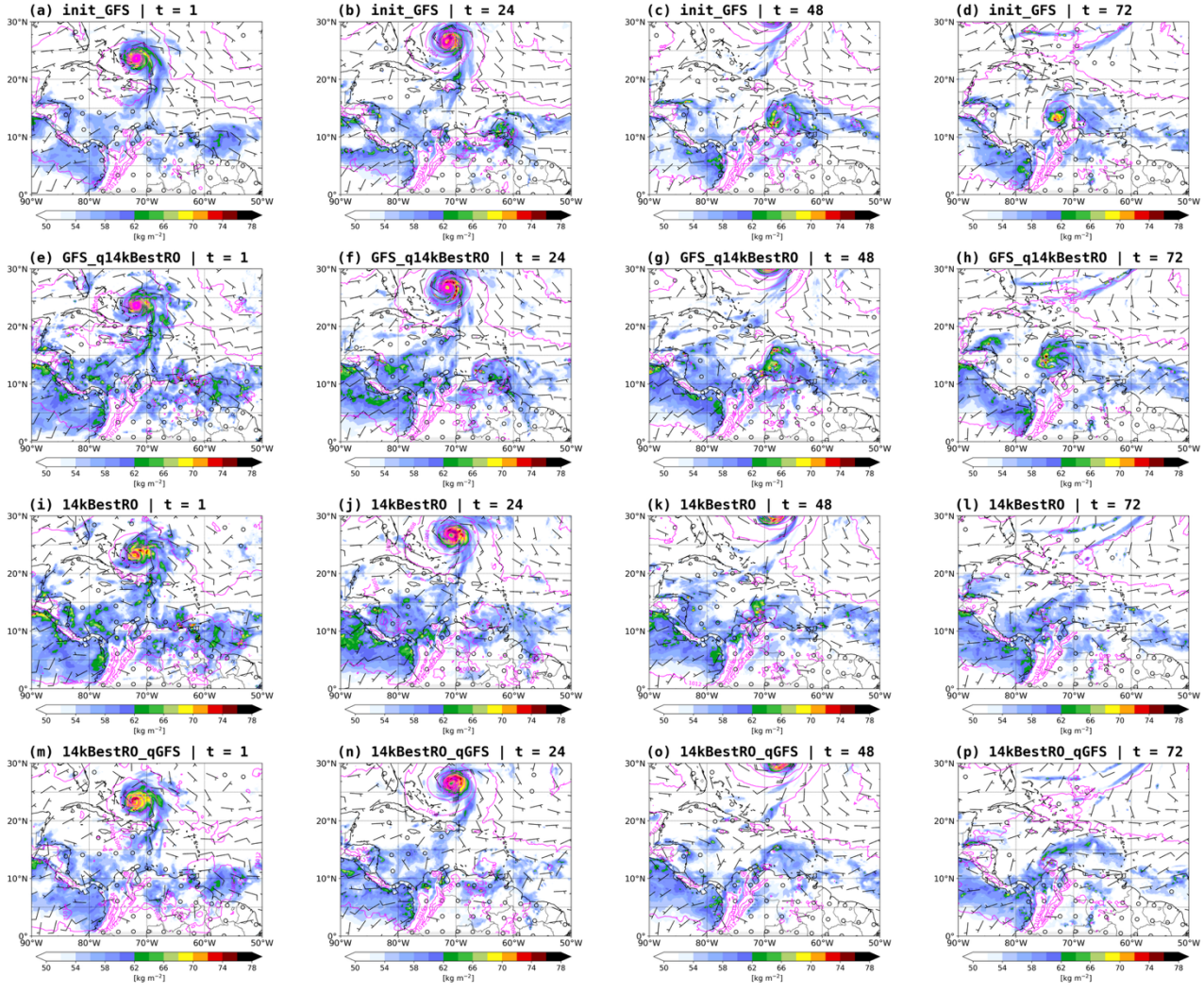

Figure 15: Snapshot of the mean sea level pressure (magenta contours; hPa), precipitable water (color-shaded; kg m^{-2}), and 10-m wind barb (black; kt) at forecast hour (a, e, i, m) t = 1 h, (b, f, j, n) t = 24 h, (c, g, k, o) t = 48 h, and (d, h, l, p) t = 72 h from (a-d) the init_GFS, (e-h) GFS_q14kBestRO, (i-l) 14kBestRO, and (m-p) 14kBestRO_qGFS experiment.

Figure 14 shows the evolution of the maximum 10-m wind speed near the low-level vortex center and the corresponding minimum sea level pressure over the forecast period. Among the experiments, init_GFS and GFS_q14kBestRO successfully predicted cyclogenesis at t = 24 h and t = 36 h, respectively. However, their subsequent evolution diverged after t = 55 h. In init_GFS, the storm continued to intensify and reached its peak intensity at t = 106 h (Fig. 14). In contrast, the storm in GFS_q14kBestRO weakened after t = 66 h as it moved westward (instead of northward, like the observed storm) into a less favorable environment, including land interaction (Figs. 15e-h).

https://doi.org/10.5194/egusphere-2026-2704
Preprint. Discussion started: 27 May 2026

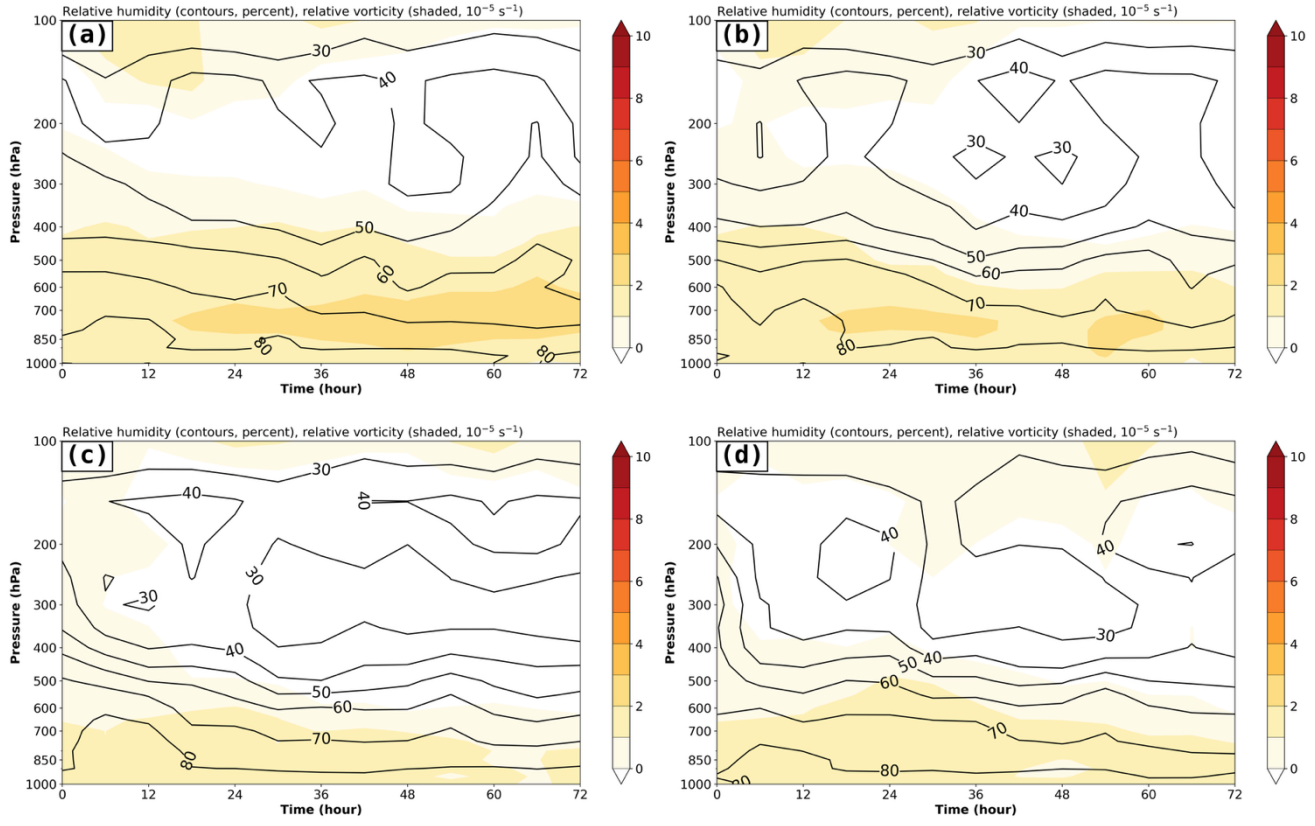

Figure 16: Time-pressure cross-sections of relative humidity (black contours; %) and relative vorticity (color-shaded; 10^{-5} s^{-1}) for (a) the init_GFS, (b) GFS_q14kBestRO, (c) 14kBestRO, and (d) 14kBestRO_qGFS experiments from forecast hour t = 0 h to t = 72 h. Both variables are azimuthally averaged within a 500-km radius of the vortex center.

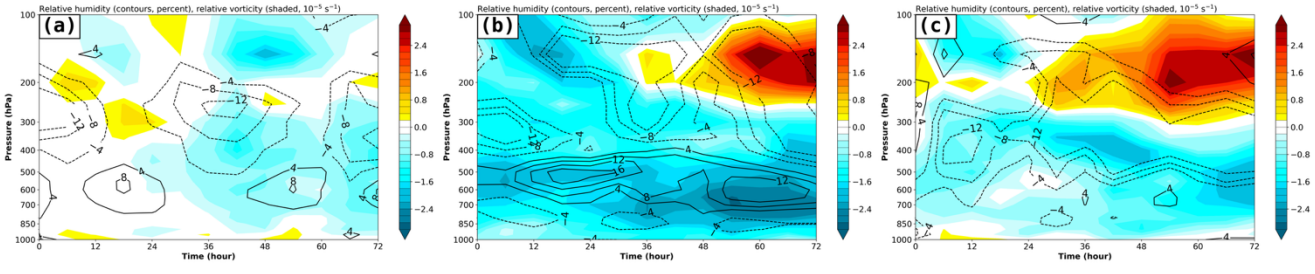

Figure 17: The differences in relative humidity (black contours; %) and relative vorticity (color-shaded; 10^{-5} s^{-1}) between (a) GFS_q14kBestRO and init_GFS, (b) 14kBestRO and init_GFS, and (c) 14kBestRO_qGFS and init_GFS from forecast hour t = 0 h to t = 72 h. Both variables are azimuthally averaged within a 500-km radius of the vortex center.

The time-height evolution of relative vorticity and relative humidity (Figs. 16-17) further illustrates these differences. Although the initial lower-tropospheric vorticity structures are identical, GFS_q14kBestRO exhibits a drier environment in the mid- to upper troposphere (200-500 hPa) compared to init_GFS (Fig. 17a). As forecast evolves, relative vorticity between 400 and

https://doi.org/10.5194/egusphere-2026-2704
Preprint. Discussion started: 27 May 2026

600 hPa becomes weaker in GFS_q14kBestRO after t = 20 h, indicating weakened vortex intensification. These results suggest that the moisture field in the 14kBestRO analysis, though better than 8kRO and 14kPoorRO, is still insufficient (or not optimally aligned with the dynamic fields) to support continued intensification of the incipient vortex. It should be noted that the operational GFS analysis assimilated considerably more non-RO data than that of 14kBestRO.

The differences between 14kBestRO and init_GFS (Fig. 17b) shows that 14kBestRO has significantly weaker relative vorticity throughout the forecast, especially below 500 hPa. The development of Hurricane Ian in init_GFS resulted in continued intensification of vorticity between 850 hPa and 500 hPa and anticyclonic vorticity between 100 and 200 hPa, from t = 36 h to t = 72 h. Interestingly, 14kBestRO possesses higher relative humidity than that of init_GFS between 700 and 500 hPa, and lower relative humidity below 700 hPa and above 500 hPa throughout the forecast. The drier low-level (below 700 hPa) is an indication that there is insufficient low-level moisture convergence because of the lack of convective development. This shows that the use of extra RO data is useful to improve the moisture analysis. Unfortunately, with the incipient vortex being too weak in the final analysis, the added mid-level moisture was insufficient to produce Ian's genesis. A successful simulation of Hurricane Ian's analysis requires improved analysis of both vorticity and humidity and proper alignment. This suggests that the failure of 14kBestRO in capturing Ian's genesis should not be attributed to RO data assimilation alone. Rather, it is related to the assimilation of non-RO data (i.e., wind observations) which are needed to capture the vorticity structure of the initial vortex.

It is well known that the development of tropical cyclone is driven by latent heat release associated with precipitation. In a conditionally unstable environment with sufficient moisture, the friction associated with the cyclonic circulation leads to low-level moisture convergence, which triggers convection. Latent heat release associated with condensation leads to upward vertical motion and low-level convergence. Through Coriolis force low-level convergence produces increased cyclonic circulation and vortex intensification, establishing a positive feedback process. This was known as the Conditional Instability of the Second Kind (CISK; Ooyama, 1982). It would be interesting to examine the precipitation evolution of GFS_q14kBestRO and ini_GFS during the 120h forecast. Figure 18 shows the total convective and non-convective precipitation within 2˚ of the vortex centers. The convective precipitation is similar between these two experiments and is generally smaller (by close to a factor of two) than the non-convective precipitation. The non-convective precipitation is smaller in GFS_q14kBestRO than in init_GFS after t = 50 h, indicating weaker latent heat release. Even though both experiments have identical dynamic fields (i.e., vorticity) at the start of the forecast, the difference in moisture distribution leads to different evolution of the vortex. As a result, the genesis of Ian in GFS_q14kBestRO occurs 12h later than that in init_GFS. This underscores the importance of the coupling between dynamic forcing and diabatic heating in tropical cyclogenesis. Although the storm in GFS_q14kBestRO weakens due to environmental constraints, it is possible that, in the absence of land interaction, further intensification could occur, suggesting that the timing and location of this coupling are also critical for a successful genesis prediction.

https://doi.org/10.5194/egusphere-2026-2704
Preprint. Discussion started: 27 May 2026

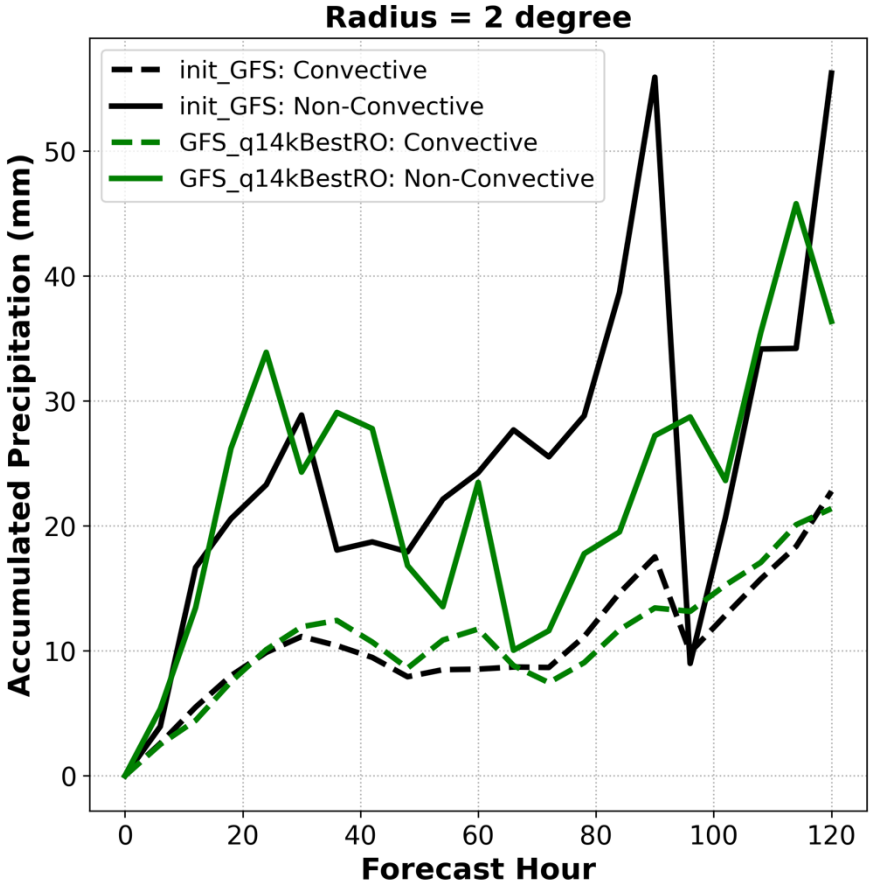

Figure 18: 1-hr accumulated non-convective precipitation (solid lines; mm) and convective precipitation (dashed line; mm) for the init_GFS (black) and GFS_q14kBestRO (green) experiments over the forecast period (t = 0 h to t = 120 h). Both variables are azimuthally averaged within a 2° radius of the vortex center.

In contrast, cyclogenesis does not occur in the 14kBestRO_qGFS experiment, despite the initially more favorable moisture field. This indicates that the incipient vortex (i.e., vorticity) in 14kBestRO is not sufficiently strong to initiate the CISK mechanism, allowing an accelerated intensification of the vortex. Indeed, there is little difference between 14kBestRO_qGFS and 14kBestRO (Fig. 14), and the disturbance dissipates after entering the Caribbean Sea (Figs. 15i-p). Although a weak closed circulation appears at t = 24 h in 14kBestRO_qGFS, precipitable water and relative humidity remain lower than in init_GFS throughout the forecast (Figs. 15 and 17b-c), confirming that improving the moisture field alone is insufficient for cyclogenesis if the initial vorticity is too weak.

In summary, the results suggest that the unsuccessful prediction of Ian's cyclogenesis in the three DA experiments stems from the inaccurate analysis of the dynamic fields (i.e., vorticity). The additional RO data from the 14kBestRO were useful in producing an improved moisture analysis. However, the assimilation of extra RO data over a 72-h period is insufficient in producing an accurate analysis of the vorticity field associated with the incipient cyclone. Genesis can be simulated if the

https://doi.org/10.5194/egusphere-2026-2704
Preprint. Discussion started: 27 May 2026

dynamic fields in 14kBestRO is replaced by that of the GFS analysis. To properly capture the vorticity structure of the incipient cyclone, additional observations (i.e., wind observations) is needed. It is possible that the assimilation of additional RO data over an extended period (much longer than 72-h) might be able to improve the analysis of the dynamic fields. This should be explored in the future.

The sensitivity experiments show that accurate analysis of both moisture and the dynamic fields are needed to capture tropical cyclogenesis, especially for the bottom-up development like Hurricane Ian (Dunkerton et al., 2009; Minamide et al., 2020). Simply improving the moisture field or the dynamic field is insufficient to initiate the positive feedback associated with the CISK process. These findings highlight the need for improved assimilation of moisture-sensitive observations and better coupling between thermodynamic and dynamic analyses to improve the predictability of tropical cyclogenesis.

6 Summary

This study evaluated the impact of GNSS radio occultation (RO) observation density and its spatiotemporal distribution on tropical cyclogenesis prediction over the North Atlantic during the 2022 hurricane season. Three data assimilation (DA) experiments, named 8kRO, 14kBestRO, and 14kPoorRO, were conducted using three RO datasets of varying amount and coverage. Among the six selected TCs, the 14kBestRO experiment produced the most skillful prediction, accurately capturing the genesis of Fiona, Julia, and Nicole, and detecting the initial, though short-lived, genesis of Gaston.

The improved performance of the 14kBestRO experiment is attributed to its denser and more uniform distribution of RO observations, particularly over the tropical and subtropical North Atlantic Ocean. The assimilation of additional profiles near incipient cyclones resulted in enhanced mid-level humidity and stronger relative vorticity, creating conditions favorable for the organization and intensification of tropical disturbances, as illustrated by Hurricane Fiona. Even though 14kPoorRO has roughly the same volume of RO profiles with 14kBestRO, its distribution is not horizontally uniform, leaving significant gaps in the tropics. The performance of 14kPoorRO (16.7%) is significantly lower than 14kBestRO (33.4%) in terms of probability of detection. These results underscore the importance of not only the number of observations, but also their spatial proximity to the developing vortices and their temporal availability during key phases of storm development. These results are consistent with Chen et al. (2020) which showed that the RO observations in the vicinity of storm are most critical in improving the prediction of tropical cyclogenesis.

Despite the assimilation of RO observations, the genesis of Hurricane Ian and Hurricane Lisa was not successfully predicted in any of the experiments. Nevertheless, the 14kBestRO experiment produced higher moisture and a slightly stronger incipient vortex for Hurricane Ian, even though it was not able to trigger cyclogenesis within the forecast period. Additional model sensitivity experiments indicate that the failure to produce Ian's genesis was mainly related to the failure to produce a sufficiently strong initial vortex, despite the assimilation of additional RO data over a 72-h period. For a shallow system, such as Hurricane Ian, additional non-RO observations are needed to accurately capture the dynamic fields. It is possible that assimilation of additional RO data over a longer (more than 72 h) period might improve the analysis of the dynamic field. To

https://doi.org/10.5194/egusphere-2026-2704
Preprint. Discussion started: 27 May 2026

trigger the cyclogenesis through the CISK mechanism, accurate analysis of both thermodynamic and dynamic fields is necessary.

The findings of this study lead to the following recommendations for future satellite observing systems:

1. Increased RO density is critical for improving analyses of the pre-genesis environment, especially in data-sparse regions such as the tropical North Atlantic Ocean.
2. A higher refresh rate is beneficial for reducing data gaps and improving the accuracy of the observed atmospheric state.

While this study focused on a single hurricane season in the North Atlantic, the approach is extensible to other ocean basins prone to tropical cyclone activity, such as the Western North Pacific, Eastern North Pacific, and Indian Ocean. Additionally, expanding this analysis to multiple seasons would allow for a more robust assessment of year-to-year variability in the relationship between RO coverage and predictive skills of tropical cyclogenesis. Future work may also explore the integration of GNSS RO with other observations, as well as the use of observing system simulation experiments (OSSEs) to inform optimal satellite constellation design and operational data assimilation strategies.

In conclusion, this study provides compelling evidence that denser and a more uniformly distributed GNSS RO observations can significantly improve tropical cyclogenesis forecasts. These findings support continued investment in next-generation RO missions and provide guidance for optimizing observational strategies aimed at improving early warnings for tropical cyclone formation.

Data availability. The NCEP GFS global analysis data (doi: 10.5065/D65D8PWK), NCEP ADP global upper air and surface weather observations (i.e., conventional data; doi: 10.5065/Z83F-N512), NCEP GDAS Satellite data (doi: 10.5065/DWYZ-Q852) were obtained from the NSF NCAR Geoscience Data Exchange platform at https://gdex.ucar.edu/. The ROMEX data were provided by UCAR COSMIC Data Analysis and Archive Center (CDAAC). The best track data for the six cyclones were obtained from the National Hurricane Center tropical cyclone reports at https://www.nhc.noaa.gov/data/tcr/index.php?basin=atl&season=2022.

Author contributions **Conceptualization:** H.-C. Lin, Y.-H. Kuo, J.-P. Weiss, J. Braun, W. Gullotta **Data curation:** H.-C. Lin, Y.-H. Kuo **Formal analysis:** H.-C. Lin, Y.-H. Kuo **Funding acquisition:** J.-P. Weiss, J. Braun, W. Gullotta **Methodology:** H.-C. Lin, Y.-H. Kuo **Project administration:** J.-P. Weiss, J. Braun **Resources:** J.-P. Weiss, J. Braun, W. Gullotta **Visualization:** H.-C. Lin **Writing – original draft:** H.-C. Lin **Writing – review & editing:** H.-C. Lin, Y.-H. Kuo, J.-P. Weiss, J. Braun, W. Gullotta

Competing interests. The authors declare that they have no conflict of interest.

https://doi.org/10.5194/egusphere-2026-2704
Preprint. Discussion started: 27 May 2026

Acknowledgements. This research is supported by the National Oceanic and Atmospheric Administration (NOAA) Science Collaboration Program Agreement under award NA23OAR4310383B. We thank NOAA NESDIS Office of Systems Architecture and Engineering for supporting this work. We would like to acknowledge high-performance computing support from the Derecho system (doi:10.5065/qx9a-pg09) provided by the NSF National Center for Atmospheric Research (NCAR), sponsored by the National Science Foundation. We also thank Mr. Christopher Barsoum from the Aerospace Corporation for providing the satellite information to construct the three RO datasets. We thank Dr. Ying Zhang, Dr. Tao Sun, and Ms. Xuewei Zhang in the NSF NCAR Mesoscale and Microscale Meteorology Laboratory for the support on the WRFDA configuration and the guidance on satellite radiance data assimilation. We greatly appreciate the science discussions with Dr. Hsu-Feng Teng from the National Taiwan University, Dr. Richard Anthes from the UCAR COSMIC, Dr. Benjamin Johnston from the UCAR CPAESS, and the UCAR COSMIC team.

References

Anthes, R. A., Marquardt, C., Ruston, B., and Shao, H.: Radio Occultation Modeling Experiment (ROMEX): Determining the impact of radio occultation observations on numerical weather prediction, Bull. Amer. Meteor. Soc., 105, E1522-E1568, https://doi.org/10.1175/BAMS-D-23-0326.1, 2024.

Barker, D., Huang, X.-Y., Liu, Z., Auligné, T., Zhang, X., Rugg, S., Ajjaji, R., Bourgeois, A., Bray, J., Chen, Y., Demirtas, M., Guo, Y.-R., Henderson, T., Huang, W., Lin, H.-C., Michalakes, J., Rizvi, S., and Zhang, X.: The Weather Research and Forecasting Model's Community Variational/Ensemble Data Assimilation System: WRFDA, Bull. Amer. Meteor. Soc., 93, 831–843, https://doi.org/10.1175/BAMS-D-11-00167.1, 2012.

Beven II, J. L., and Alaka, L.: Hurricane Nicole (AL172022). National Hurricane Center Tropical Cyclone Report, 59 pp, https://www.nhc.noaa.gov/data/tcr/AL172022_Nicole.pdf, 2023.

Blake, E. S.: Hurricane Lisa (AL152022). National Hurricane Center Tropical Cyclone Report, 21 pp, https://www.nhc.noaa.gov/data/tcr/AL152022_Lisa.pdf, 2023.

Bucci, L., Alaka, L., Hagen, A., Delgado, S., and Beven J.: Hurricane Ian (AL092022). National Hurricane Center Tropical Cyclone Report, 72 pp, https://www.nhc.noaa.gov/data/tcr/AL092022_Ian.pdf, 2023.

Cangialosi, J. P.: Hurricane Julia (AL132022, EP182022). National Hurricane Center Tropical Cyclone Report, 23 pp, https://www.nhc.noaa.gov/data/tcr/AL132022_EP182022_Julia.pdf, 2023.

Chen, S.-Y., Huang, C.-Y., Kuo, Y.-H., Kuo, Y.-R., and Sokolovskiy, S.: Assimilation of GPS refractivity from FORMOSAT-3/COSMIC using a nonlocal operator with WRF 3DVAR and its impact on the prediction of a typhoon event, Terr. Atmos. Oceanic Sci., 20, 133-154, https://doi.org/10.3319/TAO.2007.11.29.01(F3C) , 2009.

Chen, S.-Y., Kuo, Y.-H., and Huang, C.-Y.: The impact of GPS RO data on the prediction of tropical cyclogenesis using a nonlocal observation operator: an initial assessment, Mon. Wea. Rev., 148, 2701-2717, https://doi.org/10.1175/MWR-D-19-0286.1, 2020.

https://doi.org/10.5194/egusphere-2026-2704
Preprint. Discussion started: 27 May 2026

Du, X., Chu, J.-E., Jin, F.-F., and Cheung, H. M.: Global coupled dynamics of tropical easterly waves and tropical cyclone genesis, npj Clim. Atmos. Sci., 8, 125, https://doi.org/10.1038/s41612-025-01014-y, 2025.

Dunkerton, T. J., Montgomery, M. T., and Wang, Z.: Tropical cyclogenesis in a tropical wave critical layer: easterly waves, Atmos. Chem. Phys., 9, 5587-5646, https://doi.org/10.5194/acp-9-5587-2009, 2009.

Glotfelty, T., Alapaty, K., He, J., Hawbecker, P., Song, X., and Zhang, G.: The Weather Research and Forecasting Model with Aerosol-Cloud Interactions (WRF-ACI): Development, evaluation, and initial application, Mon. Wea. Rev., 147, 1491-1511, https://doi.org/10.1175/MWR-D-18-0267.1, 2019.

Halperin, D. J., Fuelberg, H. E., Hart, R. E., Cossuth, J. H., Sura, P., and Pasch, R. J.: An evaluation of tropical cyclone genesis forecasts from global numerical models, Wea. Forecasting, 28, 1423-1445, https://doi.org/10.1175/WAF-D-13-00008.1, 2013.

Hartman, C. M., Chen, X., and Chan, M.-Y.: Improving tropical cyclogenesis forecasts of Hurricane Irma (2017) through the assimilation of all-sky infrared brightness temperatures, Mon. Wea. Rev., 151, 837-853, https://doi.org/10.1175/MWR-D-22-0196.1, 2023.

Iacono, M. J., Delamere, J. S., Mlawer, E. J., Shephard, M. W., Clough, S. A., and Collins, W. D.: Radiative forcing by long–lived greenhouse gases: Calculations with the AER radiative transfer models, J. Geophys. Res., 113, D13103, https://doi.org/10.1029/2008JD009944, 2008.

Landsea, C. W.: A climatology of intense (or major) Atlantic hurricanes, Mon. Wea. Rev., 121, 1703-1713, https://doi.org/10.1175/1520-0493(1993)121<1703:ACOIMA>2.0.CO;2, 1993.

Li, Z., and Pu, Z.: Numerical simulations of the genesis of Typhoon Nuri (2008): Sensitivity to initial conditions and implications for the roles of intense convection and moisture conditions, Wea. Forecasting, 29, 1402-1424, https://doi.org/10.1175/WAF-D-14-00003.1, 2014.

Liu, H., Anderson, J., and Kuo, Y.-H.: Improved analyses and forecasts of Hurricane Ernesto's genesis using radio occultation data in an ensemble filter assimilation system, Mon. Wea. Rev., 140, 151-166, https://doi.org/10.1175/MWR-D-11-00024.1, 2012.

Majumdar, S. J., and Torn, R. D.: Probabilistic verification of global and mesoscale ensemble forecasts of tropical cyclogenesis, Wea. Forecasting, 29, 1181-1198, https://doi.org/10.1175/WAF-D-14-00028.1, 2014.

Minamide, M., Zhang, F., and Clothiaux, E. E.: Nonlinear forecast error growth of rapidly intensifying Hurricane Harvey (2017) examined through convection-permitting ensemble assimilation of GOES-16 all-sky radiances, J. Atmos. Sci., 77, 4277-4296, https://doi.org/10.1175/JAS-D-19-0279.1, 2020.

Nakanishi, M., and Niino, H.: An improved Mellor-Yamada level-3 model: its numerical stability and application to a regional prediction of advection fog, Bound. Layer Meteor., 119, 397-407, https://doi.org/10.1007/s10546-005-9030-8, 2006.

Nakanishi, M., and Niino, H.: Development of an improved turbulence closure model for the atmospheric boundary layer, J. Meteor. Soc. Japan, 87, https://doi.org/10.2151/jmsj.87.895, 2009.

NOAA National Centers for Environmental Information (NCEI) U.S. Billion-Dollar Weather and Climate Disasters. https://www.ncei.noaa.gov/access/billions/, https://doi.org/10.25921/stkw-7w73, 2025.

https://doi.org/10.5194/egusphere-2026-2704
Preprint. Discussion started: 27 May 2026

Olson, J. B., Kenyon, J. S., Angevine, W. M., Brown, J. M., Pagowski, M., and Sušelj, K.: A description of the MYNN-EDMF scheme and the coupling to other components in WRF-ARW, NOAA Technical Memorandum OAR GSD, 61, 37 pp, https://doi.org/10.25923/n9wm-be49, 2019.

Olson, J. B., Smirnova, T., Kenyon, J. S., Turner, D. D., Brown, J. M., Zheng, W., and Green, B. W.: A description of the MYNN surface-layer scheme, NOAA Technical Memorandum OAR GSL, 67, 26 pp, https://doi.org/10.25923/f6a8-bc75, 2021.

Ooyama, K. V.: Conceptual evolution of the theory and modeling of the tropical cyclone, J. Meteor. Soc. Japan, 60, 369-380, https://doi.org/10.2151/jmsj1965.60.1_369, 1982.

Pasch, R. J.: Tropical Storm Gaston (AL082022). National Hurricane Center Tropical Cyclone Report, 13 pp, https://www.nhc.noaa.gov/data/tcr/AL082022_Gaston.pdf, 2023.

Pasch, R. J., Reinhart, B. J., and Alaka, L.: Hurricane Fiona (AL072022). National Hurricane Center Tropical Cyclone Report, 60 pp, https://www.nhc.noaa.gov/data/tcr/AL072022_Fiona.pdf, 2023.

Peng, M. S., Fu, B., Li, T., and Stevens, D. E.: Developing versus nondeveloping disturbances for tropical cyclone formation. Part I: North Atlantic, Mon. Wea. Rev., 140, 1047-1066, https://doi.org/10.1175/2011MWR3617.1, 2012.

Rajasree, V.P.M., Cao, X., Ramsay, H., Núñez Ocasio, K. M., Kilroy, G., Alvey III, G. R., Chang, M., Nam, C. C., Fudeyasu, H., Teng, H.-F., and Yu, H.: Tropical cyclogenesis: controlling factors and physical mechanisms, Trop. Cyclone Res. Rev., 12, 165-181, https://doi.org/10.1016/j.tcrr.2023.09.004, 2023.

Russell, J. O., Aiyyer, A. J., White, D., and Hannah, W.: Revisiting the connection between African easterly waves and Atlantic tropical cyclogenesis, Geophys. Res. Lett., 44, 587-595, https://doi.org/10.1002/2016GL071236, 2017.

Skamarock, W. C., Klemp, J. B., Dudhia, J., Gill, D. O., Liu, Z., Berner, J., Wang, W., Powers, J. G., Duda, M. G., Barker, D. M., and Huang, X.-Y.: A Description of the Advanced Research WRF Version 4, NCAR Tech. Note NCAR/TN-556+STR, 145 pp, https://doi.org/10.5065/1dfh-6p97, 2019.

Sokolovskiy, S., Kuo, Y.-H., and Wang, W.: Assessing the accuracy of a linearized observation operator for assimilation of radio occultation data: Case simulations with a high-resolution regional analysis, Mon. Wea. Rev., 133, 2200-2212, https://doi.org/10.1175/MWR2948.1, 2005a.

Sokolovskiy, S., Kuo, Y.-H., and Wang, W.: Evaluation of a linear phase observation operator with CHAMP radio occultation data and high-resolution regional analysis, Mon. Wea. Rev., 133, 3053-3059, https://doi.org/10.1175/MWR3006.1, 2005b.

Tang, B. H., Fang, J., Bentley, A., Kilroy, G., Nakano, M., Park, M.-S., Rajasree, V.P.M., Wang, Z., Wing, A. A., and Wu, L.: Recent advances in research on tropical cyclogenesis, Trop. Cyclone Res. Rev., 9, 87-105, https://doi.org/10.1016/j.tcrr.2020.04.004, 2020.

Tao, W.-K., Simpson, J., and McCumber, M.: An ice-water saturation adjustment, Mon. Wea. Rev., 117, 231-235, https://doi.org/10.1175/1520-0493(1989)117<0231:AIWSA>2.0.CO;2, 1989.

Tao, W.-K., Wu, D., Lang, S., Chern, J.-D., Peters-Lidard, C., Fridlind, A., and Matsui, T.: High-resolution NU-WRF simulations of a deep convective-precipitation system during MC3E: further improvements and comparisons between Goddard

https://doi.org/10.5194/egusphere-2026-2704
Preprint. Discussion started: 27 May 2026

microphysics schemes and observations, J. Geophys. Res. Atmos., 121, 1278-1305, https://doi.org/10.1002/2015JD023986, 2016.

Teng, H. F., Kuo, Y. H., and Done, J. M.: Importance of midlevel moisture for tropical cyclone formation in easterly and monsoon environments over the western north Pacific, Mon. Wea. Rev., 149 (7), 2449-2469, https://doi.org/10.1175/MWR-D-20-0313.1, 2021.

Teng, H.-F., Kuo, Y.-H., and Done, J. M.: Potential impacts of radio occultation data assimilation on forecast skill of tropical cyclone formation in the western North Pacific, Geophys. Res. Lett., 50, e2021GL096750, https://doi.org/10.1029/2021GL096750, 2023.

Tewari, M., Chen, F., Wang, W., Dudhia, J., LeMone, M. A., Mitchell, K., Ek, M., Gayno, G., Wegiel, J., and Cuenca, R. H.: Implementation and verification of the unified NOAH land surface model in the WRF model, 20th conference on weather analysis and forecasting/16th conference on numerical weather prediction, pp. 11–15, 2004.

Wang, Z., Li, W., Peng, M. S., Jiang, X., McTaggart-Cowan, R., and Davis, C. A.: Predictive skill and predictability of North Atlantic tropical cyclogenesis in different synoptic flow regimes, J. Atmos. Sci., 75, 361-378, https://doi.org/10.1175/JAS-D-17-0094.1, 2018.

Yang, S.-C., Chen, S.-H., and Chang, C.-C.: Understanding the impact of assimilating FORMOSAT-7/COSMIC-2 radio occultation refractivity on tropical cyclone genesis: observing system simulation experiments using Hurricane Gordon (2006) as a case study, Quart. J. Roy. Meteor. Soc., 149, 1293-1318, https://doi.org/10.1002/qj.4455, 2023.

Zheng, Y., Alapaty, K., Herwehe, J. A., Del Genio, A. D., and Niyogi, D.: Improving high-resolution weather forecasts using the Weather Research and Forecasting (WRF) Model with an updated Kain-Fritsch scheme, Mon. Wea. Rev., 117-3, 883-860, https://doi.org/10.1175/MWR-D-15-0005.1, 2016.